Progress Report under IAEA Research Contract №15370

Title of Project: «*Investigation of PWR and VVER Fuel Rod Performances under High Burnup Using FEMAXI & PAD Codes*»

Title of Report

FUEL ROD PERFORMANCE EVALUATION OF CE 16×16 LTA OPERATED AT STEADY STATE USING TRANSURANUS AND PAD CODES

Host organization: "Nuclear Fuel Cycle" Science and Technology Establishment (NFC STE), National Science Center "Kharkov Institute of Physics and Technology (NSC KIPT)

Contractor:

Director, NFC STE NSC KIPT

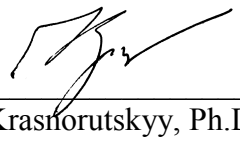

V. Krasnorutskyy, Ph.D.

Chief Scientific Investigator

O. Slyeptsov, Ph.D.

Reported period: October 21, 2008 – November 30, 2009

KHARKOV 2009

Revision History

Revision	Content of Change	Author	Date
0	Initial edition	O. Slyeptsov	November 2009

TABLE OF CONTENTS

List of abbreviation 4
List of tables 5
List of figures 5
Executive summary 7
1. INTRODUCTION 9
1.1 Background 9
1.2 Limits of Applicability 10
2. CODES DESCRIPTION 11
2.1 Code PAD (ver. 10.5.2) 11
2.2 Code TRANSURANUS (v1m1j09) 16
3. DATA DESCRIPTION FROM US-PWR 16×16 LTA EXTENDED BURNUP DEMONSTRATION PROGRAM 17
3.1 Introduction 17
3.2 Rod Design and Fabrication 17
3.3 Reactor Operational Data 19
3.4 Irradiation History Data 19
3.5 Rod Data for Assessment 20
3.6 General Assumptions Used 20
4. PAD FUEL PERFORMANCE PREDICTION 22
4.1 Introduction 22
4.2 Fuel Rod Burn-ups 22
4.3 Cladding Corrosion 24
4.4 Fuel Densification and Swelling 26
4.5 Cladding Creep 29
4.6 Fuel Rod Growth 31
4.7 Fuel Rod Void Volume 31
4.8 Fission Gas Release and Rod Internal Pressure 32
4.9 Conclusion 34
5. TRANSURANUS FUEL PERFORMANCE PREDICTION 35
5.1 Introduction 35
5.2 Fuel Rod Burn-ups 35
5.3 Cladding Corrosion 36
5.4 Fuel Densification and Swelling 37
5.5 Cladding Creep 39
5.6 Fuel Rod Growth 42
5.7 Fuel Rod Void Volume 42
5.8 Fission Gas Release and Rod Internal Pressure 44
5.9 Conclusion 46
REFERENCES 48
ACKNOWLEDGEMENTS 51
APPENDIX A 52
APPENDIX B 57

List of abbreviation

ADU	Ammonium DiUranate (fuel pellet manufacturing process)
BE	Best Estimate
BOC	Beginning- Of-Cycle
BOL	Beginning-Of-Life
BWR	Boiling Water Reactor
BU	Burnup
CE	Combustion Engineering
CRCD	Center for Reactor Core Design
E.ON	E.ON is Germany energy company
E110	Zr-1%Nb alloy marketed by Russian corporation “TVEL”
FA	Fuel Assembly
FR	Fuel Rod
FGR	Fission Gas Release
GWD/MTU	Giga-Watt Day per Metric Tonne of initial Uranium metal
HBS	High Burnup Structure
IAEA	International Atomic Energy Agency
IDR	Integrated Dry Route powder conversion process
IFPE	International Fuel Performance Experiments
ITU	Institute for Transuranium Elements
LHR (LHGR)	Linear Heat Generated Rate
LTA	Lead Test Assembly
LWR	Light Water Reactor
MOX	Mixed-Oxide $(U,Pu)O_2$ fuel
MWD/MTU	Mega-Watt Day per Metric Tonne of initial Uranium metal
ND	Nominal Dimension
NEA	Nuclear Energy Agency
OECD	Organisation for Economic Co-operation and Development
PAD	Fuel rod design code developed by Westinghouse
RIP	Rod Internal Pressure
PWR	Pressurized Water Reactor
SNRCU	State Nuclear Regulatory Committee of Ukraine
VVER	Russian-designed pressurized water reactor
TU	TRANSURANUS code developed by ITU
WEC	Westinghouse Electric Company
WSE	Westinghouse Sweden
UNFQP	Ukraine Nuclear Fuel Qualification Programme
US NRC	United State Nuclear Regulatory Commission
ZIRLO	Low-corrosion zirconium alloy marketed by Westinghouse

List of tables

Table 3-1. Design Specifications for ANO-2 Full-Length Fuel Rods Used in LTAs .. 18
Table 3-2. Reactor Power and Thermal Hydraulic Design Data 19
Table 3-3. Fuel Rod Data for Assesments 21
Table 4-1. Measured and PAD Predicted Peak Oxide Thickness..... 24
Table 4-2. Measured and PAD Predicted Cladding Strain 29
Table 4-3. Measured and PAD Predicted Fuel Rod Void Volume Change..... 32
Table 5-1. Measured and TU Predicted Peak Oxide Thickness 36
Table 5-2. Measured and TU Predicted Cladding Strain 39
Table 5-3. Measured and TU Predicted Fuel Rod Growth 42
Table 5-4. Measured and TU Predicted Fuel Rod Void Volume Change 43
Table 5-5. Measured and TU Predicted Fission Gas Xe/Kr Ratio..... 44

List of figures

Figure 4-1. PAD predicted fuel rod burnup versus measured. 23
Figure 4-2. Measured and PAD predicted fuel rod burnup for TSQ002 fuel rod. 23
Figure 4-3. Measured and PAD predicted axial oxide thickness variation for TSQ002 fuel rod… 25
Figure 4-4. Measured and PAD predicted axial oxide thickness variation for TSQ022 fuel rod… 26
Figure 4-5. Measured and PAD predicted fuel pellet density change versus burnup… 27
Figure 4-6. Measured and PAD predicted fuel swelling versus burnup… 27
Figure 4-7. Measured and PAD predicted fuel swelling of fuel rods operated in different cores of PWR, VVER (1000&440 and BR3 reactor… 28
Figure 4-8. EOL measures and PAD predicted cladding outer diameter change for TSL_095/176 fuel rods…..... 30
Figure 4-9. EOL measured and PAD predicted cladding outer diameter change for TSQ002 fuel rod…..... 30
Figure 4-10. EOL measured and PAD predicted cladding outer diameter change for TSQ022 fuel rod…..... 31
Figure 4-11. EOL measured and PAD predicted fission gas release… 33
Figure 4-12. EOL measured and PAD predicted rod internal pressure… 33
Figure 5-1. TU predicted fuel rod burnup versus measured…..... 36
Figure 5-2. Measured and TU predicted fuel pellet density change versus burnup…..... 38
Figure 5-3. Measured and TU predicted fuel swelling versus burnup… 38
Figure 5-4. Measured and TU predicted cladding outer diameter change at EOL, cold for the fuel rods with solid pellets… 40
Figure 5-5. Measured and TU predicted cladding outer diameter change at EOL cold for the fuel rods with annular pellets… 41
Figure 5-6. TU predicted fuel rod void volume change versus measured… 43

Figure 5-7. TU predicted fission gas release versus measured 45
Figure 5-8. Measured and TU predicted FGR versus fuel rod burnup …..... 45
Figure 5-9. EOL measured and TU predicted rod internal pressure… 46

Executive summary

The report performed under IAEA research contract №15370 describes the results of fuel performance evaluation of PWR fuel rods operated at steady state up to discharge burnup of ~60 GWD/MTU using the codes of TRANSURANUS designed by ITU and PAD designed by Westinghouse. The experimental results from *US-PWR 16×16 LTA Extended Burnup Demonstration Program* presented in the IFPE database of the OECD/NEA have been utilized for assessing the codes themselves during simulation of such properties as rod burnup, cladding corrosion, fuel densification and swelling, cladding irradiation growth and strain, FGR and RIP.

The results obtained by PAD showed that the code properly simulates rod burnup, cladding irradiation growth and cladding oxidation with Standard Zr-4 material. The calculated burnup values along the fuel stack vary within ± 5% of the rod average burnup. The predicted values of the rod axial growth are (0.88-0.94) % and within the measured ones obtained in the burnup range of (50 – 60) GWD/MTU. With allowance made for probability of crud deposition and hot channel hydraulic diameter variation, the axial distribution of oxide layer is predicted well. For the nominal rod dimensions and operation conditions, the calculated peak oxide thickness is slightly overestimated based on the BE corrosion model parameters.

The WEC fuel swelling and densification model together with the US NRC one, which is incorporated in the code, were used to assess the change in fuel pellet density ($\Delta\rho$) and fuel volume ($\Delta V_F/V$) vs. burnup as well as the rod void volume change, $\Delta V_V/V$, and the cladding outer diameter (OD) variation along the fuel stack. The obtained results show:

- within the measurement uncertainty the calculated values $\Delta\rho$, which are based on both the WEC and the US NRC models, agree with the measured ones for solid pellets and are slightly overestimated for annular pellets, when the NRC model with resinter fuel density change of (2.25÷2.75) % T.D. was used;

- the predicted $\Delta V_F/V$ values obtained using the WEC model correlate well with the measured for the two fuel pellet types. The US NRC model show an average 1.4% overestimation, when the fuel pellets reaches the burnup of 63 GWD/MTU;

- in the case, when the WEC model is used, the predicted $\Delta V_V/V$ values are underestimated by 5%, as a maximum, for FRs with solid pellets and are a 1% overestimation for the FR with annular pellets. The reduction resinter fuel density change up to 2.25 % T.D. results in decreased difference between the predicted and measured data for rods with solid pellets and causes the opposite effect for FR with annular pellets;

- integrally, the axial variation of cladding OD is predicted well by PAD code based on the BE rod model parameters and rod ND. The data, which were calculated using the US NRC model with the resinter fuel density change of 2.25 % T.D., are the bounding for the measured, which have been obtained for the FRs with characterized and uncharacterized cladding and pellets.

The predicted FGR based on the BE gas release model parameters is overestimated by 0.36 % on the average at the rod average burnup of ~ 50 GWD/MTU. The FGR of 1.5 % is predicted by PAD for the examined rods with the high burnup of ~ 58 GWD/MTU. The calculated RIP values bound the ones obtained for rods with discharge burnup up to ~52 GWD/MTU. As burnup grows, the predicted RIP values increase and they are an overestimation with the maximum value of 0.5 MPa at the high burnup of ~ 58 GWD/MTU.

The simulation of the FR performances was done by TRANSURANUS code using the standard code model for PWR fuel with the cladding material properties for Zr-4 alloy (MATPRO) and fission gas release model *URGAS* taking into account the athermal gas release from the fuel high burnup structure. To account for the impact of fuel relocation on FR performance changes, the *FRAPCON*-3 relocation model was turned on.

The rod burnup calculations showed that the predicted values are underestimated by ~ 3 % on the average. When the rod burnup increases, the cladding growth prediction varied from 1.05 % to 1.17 % and these values are at the upper bound of the measured. The predicted peak oxide thicknesses are underestimated by 25 mkm as a minimum.

Simple empirical model of fuel densification with different values of pellet porosity at the end of sintering, from 2.0 % to 1.0 %, and burnup at which sintering has stopped, (5÷12) GWD/MTU, was used to assess the change of the fuel volume, the pellet density, the rod void volume and the cladding deformation. The obtained results evidence:

- within the measurement uncertainty the $\Delta\rho$ values calculated using the minimum value of fuel resinter density change agrees with the measured for solid and annular pellets at burnup up to 60 GWD/MTU. A 0.7 % underestimation, as a maximum, takes place at burnup up to 57 GWD/MTU, when the maximum pore removable value was used;

- integrally, the predicted values $\Delta V_F/V$ are in satisfactory agreement with the measured. The use of the maximum fuel resinter density change provides the best agreement between the predicted and measured data for both fuel pellet types;

- for both fuel rod designs the predicted $\Delta V_V/V$ value is underestimated by half with respect to the measured;

- for the rod ND the calculated cladding OD axial variation is predicted well by TU code for FRs with different fuel pellet types. Taking into account the underestimation of oxide thickness, the use of the maximum fuel resinter density change in the model provides satisfactory agreement between the predicted and the measured values. The same result is reached in a case, when the minimum fuel resinter density change together with the axial anisotropy factor for densification of 0.1 is used.

A sharp increase in fission gas release at the rod burnup higher than 40 GWD/MTU is predicted by the code and this is due to athermal gas release from the HBS. For the rod average burnup of ~ 50 GWD/MTU the estimated FGR based on the nominal value of threshold burnup, BU_{th}, is overestimated by 1.5 % on the average. This difference decreases twofold, when the threshold burnup increases by 10% from the nominal. Based on the value of $1.1\times BU_{th}$ the FGR for the rod average burnup of ~ 57 GWD/MTU is predicted in the range of (1.5÷1.9) %.

The predicted RIP values depend on fuel swelling and densification model parameters and they are on the lower boundary of the measured area for the standard full-size fuel rods and are overpredicted by 0.2 MPa for the rods with annular pellets.

1. INTRODUCTION

1.1 Background

Very high burn-ups allow a utility increased flexibility in choosing an optimal combination of cycle length and refueling fraction. Although there may be some countries in which back-end concepts and strategies are already fixed, and where flexibility for increasing burn-ups may be limited, for the majority of utilities the motivation for adopting very high burn-up cycles is potentially very strong. However, in some circumstances, very high burn-ups reduce fuel cycle costs and this provides significant economic and operational benefits for utilities.

The past history of burn-up evolution has been characterized by a long process of incremental improvements based on a gradually increasing operational and experimental database [1]. The experimental results obtained for BWR, PWR and VVER fuel rods operated in different environments helped improve the understanding of FR failure mechanisms, which require special changes in the FA and FR design, fabrication processes and in-reactor operating procedures [2].

High efficiency and reliability of the fuel rod, that is ensured by the integrity of the cladding under both steady-state and transient operation conditions, is a basic requirement for the safe operation in power reactors [3, 4]. In order to guarantee that the rod integrity will not be violated under onerous operating conditions the qualified fuel modeling codes are used. A great number of fuel codes, such as TRANSURANUS [5], FRAPCON-3 [6], FEMAXI-V [7], FALCON [8], PINw99 [9] and others, have been developed to simulate FR performances with different fuel types and cladding materials. Some of them, like TRANSURANUS and FRAPCON-3 codes, are widely used by various research centers as well as nuclear safety authorities. Moreover, the TRANSURANUS code is also being used by different industrial companies (E.ON Kernkraft GmbH, WSE).

In safety analysis of core reloads, the fuel rod design codes and corresponding methodology developed by fuel vendors are used. Thus, the codes START-3 and TOPRA-2 are used for the Russian FRs operated in VVER-1000 & 440 cores [10, 11]. For PWR units designed by Westinghouse, the code PAD and FR design methodology are utilized [12, 13]. This methodology was expanded for VVER-1000 fuels supplied by WEC for Temelin Unit-1 & 2. In the framework of UNFQP, the WEC design code PAD and methodology was transferred for CRCD and successfully applied for safety substantiation for W LTAs use in the VVER-1000 mixed core of the South-Ukraine (SU) Unit-3 [14]. Now this FR design methodology is utilized for safety analysis of W FA reload batches for SU NPPs.

In the framework of the IAEA Coordinated Research Project FUMEX-III [15], the present work is aimed at assessing the prediction capability of the TRANSURANUS and the PAD* codes in simulating burn-up, cladding oxidation, FGR, RIP, cladding deformation (creep-down and growth), fuel swelling and densification, rod void volume for LWR fuel rods operated at steady-state up to burnup of ~ 60 GWD/MTU, based on the experimental data from *US-PWR 16×16 LTA Extended Burnup Demonstration Program* presented in the IFPE database of the OECD/NEA [16].

* Results obtained by the PAD code are part of the code validation report for SNRCU.

1.2 Limits of Applicability

The results presented in the Report were performed under IAEA Research Contract №15370 and describe the fuel performance evaluation of CE 16×16 LTA fuel rods, which were operated in ANO-2 PWR for five cycles up to discharge burnup in the range of (50 - 60) GWD/MTU.

The simulation of fuel rod behavior at steady-state operation was carried using the codes of TRANSURANUS (v1m1j09) and PAD (version 10.5.2).

The TRANSURANUS code was utilized in accordance with Software Licensing Agreement №13302*.

The PAD code was used in the frame of the UNFQP licensing agreement on Technology Transfer.

The calculation results are valid only for the examined rods and for the FR model parameters and assumptions described in the Report.

* The Software Licensing Agreement between the European Atomic Energy Committee (EUROATOM) and CRCD is pending signing.

2. CODES DESCRIPTION

A brief description of codes application is presented in this chapter. Since the TU fuel rod models and numerical algorithms were widely presented and published at different international conferences and in scientific journals [17-32], the information mostly focused on the PAD code.

2.1 Code PAD (ver. 10.5.2)

The PAD code developed by Westinghouse is the principal design tool for evaluating fuel rod performance [12]. This computer code iteratively calculates interrelated effects of temperature, pressure, cladding elastic and plastic behavior, fission gas release, and fuel densification and swelling as a function of time and linear (axial) power during steady-state operation and transient events (Condition I and II).

PAD evaluates the power history of a fuel rod as a series of steady-state power levels with instantaneous jumps from one power level to another. The length of the fuel stack is divided into several axial segments, between 5 and 49, and each segment is assumed to operate at a constant set of conditions over its length. Fuel densification and swelling, cladding stresses and strains, temperatures, burnup and fission gas releases are calculated separately for each axial segment and the effects are integrated to obtain the overall FGR and resulting internal pressure for each time step.

The fuel pellet, both of solid and annular types, is taken as a cylinder with allowances for dishing, edge chamfering and pellet chipping. For purposes of evaluating thermal expansion, fuel densification and swelling, and fission gas release, the fuel pellet is divided into ten equal-volume concentric rings with each ring assumed to be at its average temperature during a given time step. Axial and radial thermal expansion, swelling and densification are determined over the entire fuel rod to determine the length of the fuel column and evaluate the void volumes required to compute the internal gas pressure.

The PAD model is applicable on a best estimate basis for evaluations of pressurized and non-pressurized fuel rods within the following range of parameters:

- enrichment 0.75 to 9.0%;
- initial (geometrical) fuel density $\geq$ 92.5% T.D.;
- fuel type: UO_2, $(U\text{-}Pu)O_2$, $UO_2\text{-}Gd_2O_3$, $UO_2(ZrB_2)$;
- rod average LHR up to ~30 kW/m (9 kW/ft);
- FR peak power up to ~56 kW/m (17 kW/ft);
- FR average burnup $\leq$ 62 GWD/MTU;
- backfill gas type – Helium, Air and gas mixture;
- cladding material type – stainless steel (SS), standard Zircalloy-4, improved (low tin) Zircalloy-4, Zr-1%Nb alloy (ZIRLO^{TM}).

The PAD fuel rod models for calculating fuel temperature distributions, thermal expansion, FGR and RIP, fuel swelling and densification, cladding stresses and strains have been developed based on the numerical experimental data and were verified and accepted by the SU NRC (TAC № MA2086, 12.03.2000).

Below the brief description of PAD models are presented.

- **Thermal Model**

The PAD Thermal model was developed to calculate the following:

***Core Coolant and Cladding Surface Temperature*:** within a single closed-channel the coolant temperature rise is calculated based on the coolant mass flow rate and the axial power distribution. The Steam Tables [33] are used to calculate the bulk coolant temperature.

The cladding surface temperature is determined with consideration of corrosion effects and the possibility of local boiling. Under forced convection the cladding surface temperature is calculated using the Dittus-Boelter film heat conductance [34]. Under nucleate boiling, the cladding surface temperature is calculated using the maximum of either (i) parallel combination of the Thom film heat conductance and the heat transfer path for a clean surface, or (ii) the Tong heat conductance for a crudded surface. It is assumed that once the crud is deposited, it is to be retained for the life of the rod.

***Cladding Corrosion*:** the cladding oxide thickness (or weight gain in mg/dm^2/day) is determined using one of several corrosion models, which are selected by cladding material type.

For the cladding made from zirconium alloys, the corrosion model was developed based on the measured oxide thickness for rods from a variety of plants over a range of peaking factors, rod burnup, plant conditions including up-rated powers and high temperatures, and primary system chemistry (pH control). The PAD best estimate corrosion model calculates the circumferential–average oxide thickness on the cladding. The out-of -reactor (thermal) corrosion rate for the post-transition phase is a base equation. The additional multipliers taking into account the effects of fast neutron flux, zirconium alloy type, operation time- and boiling-dependant lithium concentration in the coolant on the increase cladding oxide thickness, are applied to the base equation.

***Oxide-Metal Ratio*:** in the PAD, the oxide-metal ratio accounts for the loss of cladding thickness due to corrosion. The oxide-metal ratio is then used to reduce the cladding outside diameter to account for the loss of cladding wall due to corrosion.

***Cladding Hydrogen Pickup*:** the hydrogen pickup is a direct function of the cladding oxide thickness. In the PAD, there are some hydrogen pickup models for the cladding made from different zirconium alloys. These models were developed based upon fuel cladding and thimble tube data points which had oxide thickness up to ~ 80 mkm.

***Cladding Temperature Drop*:** the temperature drop through the cladding is a function of cladding thickness and thermal conductivity of the cladding. The thermal conductivity of the cladding is the linear function of temperature. The average cladding temperature is used to determine creep rates and thermal expansion.

***Thermal Conductivity of Gas Mixtures*:** the general relationship to calculate the thermal conductivity of a monatomic gas mixture is taken from Brokaw [35]. The thermal conductivity of xenon and krypton were fit to the correlated data of Gandhi and Saxena [36]. It is assumed that fission gas is comprised of 85 percent of xenon and 15 percent of krypton. The thermal conductivity for helium is based on the results presented by Tsederberg [37]. This empirical equation was developed as a function of pressure and temperature based on measured data.

***Pellet-Cladding Gap Temperature Drop*:** the surface temperature of the fuel pellet accounting for the temperature of the cladding inside surface plus temperature drop across the pellet-cladding gap.

The PAD code contains several options for determining the gap conductance, which accounts for thermal conductivity of the gas mixture, gas pressure, fuel-to-clad contact pressure, diametral gap value as well as the cladding inside and pellet roughness.

The gap size is determined from an iterative process where the temperatures of the fuel and cladding are used to determine their thermal expansion, which in turn influence the size of the

fuel/clad gap. The hot fuel diameter is determined by summing the expanded diameter of ten individual fuel rings. The average temperature for each ring is used under expansion calculation. The radial increments are summed for all of the rings to obtain an overall expansion. Likewise, in the axial direction, the change in the height of each radial node due to temperature is calculated. When swelling and/or densification occur, appropriate changes to the respective radius and segment lengths are included.

***Temperature Drop through the Fuel*:** the radial temperature drop through a solid or annular fuel pellet is determined from an integral equation which includes fuel centerline and surface temperature, rod average power and radial power depression factor.

The radial power distribution (and the resulting radial power depression factor) in the PAD code is a function of enrichment and fuel burnup. These distributions are calculated for each axial segment by a parabolic fit of data, which are tabulated as function of burnup for U^{235} enrichments. The form of the UO_2 thermal conductivity model is taken from [38].

- **Fuel Swelling and Densification Models**

Fuel swelling and densification (pore removal) are independent physical phenomena, which occur simultaneously but at different rates. The PAD model which considers these phenomena consists of two radial regions: one region below 1200 °C and another above 1200 °C. Fission gas swelling takes place only above 1200 °C, but solid swelling takes place in both regions.

The WEC solid swelling and densification model has been developed using fuel density change data and in-core stack height data by empirical densification rate constants in the fuel volume change equation [39]. The basis equation includes two terms, which describes (i) the fission product swelling and (ii) densification contribution to the total fuel volume change ($\Delta V/V$). The constants for solid fission product swelling rate and densification rate were developed based on the fuel density change vs. sintering temperature.

There is an additional fuel densification model, referred as NRC [40], which is utilized by the PAD code. This model is used, when the fuel fabricated using a process different from the Westinghouse ADU conversion process (e.g., IDR), and the WEC densification model for the maximum densification is not applicable. According to the requirements of fuel manufacturing, the fuel is fabricated to a resinter test specification; that is, the density change of as-built fuel pellets subjected to a resinter test must fall within certain limits. The value of fuel resinter density change (measured in % T.D.) is used by NRC fuel swelling and densification model.

- **Cladding Creep Model**

PAD calculates steady-state circumferential and axial cladding strains using isotropic constitutive equations and empirical corrections for Zircaloy anisotropy to relate diametral creepdown to an effective stress (σ_{eff}).

The base PAD in-reactor cladding creep determines the total effective strain rate ($\Delta\varepsilon_{tot}$) by adding together the terms for thermal, irradiation and growth, which are calculated for each time step.

The equations for the thermal and irradiation creep rates were developed with account for the σ_{eff} and midwall hoop stress values, midwall temperature, cladding material properties and fast neutron flux (E > 1 MeV).

The axial growth rate is determined by evaluating the cladding length change ($\Delta L/L$) between time steps.

For various cladding types the calculated thermal and irradiation creep rates are multiplied by calibration factors.

- **Cladding Growth Model**

The PAD cladding growth model has been developed by regression analysis of peripheral rod growth data from assemblies irradiated in the Zion, Surry and Trojan reactors. These data cover the high levels of fast neutron fluence, which are used in the PAD growth model.

The function defining the irradiation-induced cladding elongation vs. fast neutron fluence, which was built for the FRs made from standard Zr-4 cladding material, is a base equation to calculate the BE cladding irradiation growth. The calibration coefficients used in this equation define the type of cladding material.

The fast neutron fluence vs. FR burnup is internally calculated by PAD using the conversion coefficients. These coefficients were developed for the different FA types designed to operate in PWR and VVER cores.

- **Fission Gas Release Model**

The PAD fission gas release model, which is based on a fission gas production rate of 30 atoms per 100 fissions, separates fission gas release into two additive components: low temperature (LT) release and high temperature (HT) release.

The FGR_{LT} model is an empirical correlation which accounts for fission gas release fractions (R_{LT}) due to knockout and recoil processes. The R_{LT} value depends directly on the local burnup.

The FGR_{HT} model is based on concepts drawn from mechanistic models of high temperature gas release through interlinking of grain edge fission gas bubbles. In these models, fission gas produced in the interior of the fuel grains migrates to the grain boundaries by diffusion or grain boundary sweeping, depending on the local fuel temperature. Fission gas bubbles form on the grain boundaries and a saturated gas bubble density develops on the grain edges as irradiation continues. Eventually the grain edge bubbles interlink and the fission gas stored in the bubbles is vented to the fuel rod void volume. An equilibrium release rate is established such that the net gas release rate equals the fission gas production rate. Based on the above the fission gas release fractions (R_{HT}) is defined in terms of burnup thresholds, referred as release equal production (REP) and incubation (INC). The REP and INC burn-ups are defined as functions of the local temperature by pairs of burnup and temperature values. (It is noted, that the boundary values of burnup and temperature, as the BE ones, were developed based on a numerical FGR data from pressurized and unpressurized fuel rods).

For steady-state operation the total fraction FGR to the fuel rod void volume is obtained by adding the R_{LT} and R_{HT}.

The PAD transient FGR model is a multiplicative factor ($f(\tau)$) on the steady-state high temperature fission gas release R_{HT}.

The time and temperature dependence of $f(\tau)$ is given by the analytic solution for the diffusion of the fission gas stored in a fuel grain to the grain boundary. The assumption of a spherical grain and gas diffusion constant from [41] are used to calculate the factor $f(\tau)$.

An additional adjustment to the transient fission gas release model has been made to match the high-burnup transient FGR data. This adjustment increases the predicted transient gas release for local burn-ups greater than 35 GWD/MTU. For this purpose, a multiplier, which linearly increases with burnup, when the local burnup exceeds 35 GWD/MTU, is used.

- **Rod Internal Pressure and Void Volume**

In the PAD code the rod internal pressure of the gas mixture is calculated using the Peng-Robinson equation of state (EOS). Under pressure calculation the nitrogen and oxygen in the gas mixture are assumed to react with and be absorbed by the cladding and do not contribute to the RIP value.

The various FR volume components and corresponding temperatures used in the EOS are computed for each axial fuel segment and the plenum. The following volumes are included in the FR void volume: pellet dish plus chamfer volume; fuel-to-clad gap volume; inlet and outlet plenum volumes (taken without spring volume, fuel stack support spacer volumes); surface roughness volume (it is assumed to be constant during operation); open porosity volume and radial crack volume.

The radial crack volume is the difference between the linear and the areal calculation of the pellet thermal expansion.

The open porosity volume is calculated as a function of initial fuel density and fuel temperature at power. For fuel pellets manufactured using the ADU technology, the calculation used the WEC open porosity-density correlation at room temperature. For fuel manufactured by the technology, which differs from ADU conversion process (e.g. IDR), the as-fabricated open porosity is defined by fuel vendor.

2.2 Code TRANSURANUS (v1m1j09)

The TRANSURANUS code developed at the Institute for Transuranium Elements is a computer program for thermal and mechanical analysis of fuel rods operated in different type of nuclear reactors: BWR, HBWR, PWR, VVER and FBR.

The last code version of TU(v1m1j09) [17] allows the simulation of FR performances under steady-state operation condition, transient events (related with power ramp), LOCA accident condition, as well as a wide range of different situations, as given in experiments. The analysis can be performed in two different versions: deterministic and statistical.

The fuel rod performances such as fuel densification and swelling, cladding stresses and strains, temperatures, burnup and fission gas releases along the fuel rod are calculated by the TU code for each axial segment and then are integrated to obtain the resulting RIP for each time step operation. The FR length is divided into several axial segments (slices), up to 40, when each fuel segment is assumed to operate at a constant set of conditions over its length. For specific requirements, the length of each slice can vary along the fuel rod.

Two fuel pellet types, solid and annular, are processed by TU as a cylinder. The pellet dishing, edge chamfering and cracks are considered as a rod void volume. To evaluate precisely the fuel thermal expansion, the fuel densification, the temperature, burn-up and fission elements distribution in the radial direction, the "pellet-gap-cladding" structure is divided on coarse and fine zones, maximum 20 each.

The code has a comprehensive material data bank for different types of fuel (oxide, mixed oxide, carbide and nitride fuels) and cladding materials (Zircalloy-2; Zircaloy-4; Zr-1%Nb (E110, ZIRLO); stainless steels) as well as for several different coolants (water in liquid and boiling/evaporated states; gas (He) atmosphere; Sodium, Potassium, Lead, Lead-Bismuth eutectic and Sodium(70%) / Potassium(30%) in liquid states).

All physical models included in the TU(v1m1j09) code, such as fuel thermal and irradiation-induced densification and swelling due to solid and gaseous fission products; oxygen, Pu and other fission products distribution in the pellet (*TUBRNP* block); pellet cracking and relocation (modified *FRAPCON-3* model); fission gas release (*URGAS* model, *HBS* model); creep, plasticity, volume changes during phase transitions, formation and closure of central void and treatment of axial friction forces were developed based on numerical experimental data at an OECD/NEA-CSNI/IAEA organized and sponsored by the IAEA in the form of a coordinated research programs for D-COM, FUMEX-I, FUMEX-II.

3. DATA DESCRIPTION FROM US-PWR 16×16 LTA EXTENDED BURNUP DEMONSTRATION PROGRAM

In this chapter the summary of the *US-PWR 16×16 LTA Extended Burnup Demonstration Programme* as abstracted from the IFPE database of the OECD/NEA [16] as well as the fuel rod data, which were used to assess the fuel performance prediction on the basis of the TU(v1m1j09) and PAD codes, are presented.

3.1 Introduction

The US-PWR 16×16 LTA extended burnup demonstration program was conducted during the 1980s. The U.S. Department of Energy sponsored the Program with ABB Combustion Engineering and Energy Operations, Inc. to improve the use of PWR fuel. The scope of this Project was to develop more efficient fuel management concepts and an increase in the burnup of discharged fuel.

Two CE 16×16 LTAs consisting of different FR designs were irradiated in the Arkansas Nuclear One, Unit 2 reactor (ANO-2, PWR). One of the assembly, referred as D039, was irradiated for three cycles and achieved a burnup of 33 GWD/MTU. The other one, referred as D040, was irradiated for five cycles and achieved a burnup of 52 GWD/MTU.

Both poolside (nondestructive) and hot cell (destructive) post irradiation examinations of selected rods from the two LTAs were conducted. Poolside examinations of the LTAs included visual inspection, dimensional measurements, eddy current testing (ECT), and waterside corrosion thickness measurement.

Hot cell fuel rod PIE included void volume measurements, fill gas analyses, cladding visual inspections, dimensional measurements, neutron radiography, and gamma scanning. Fuel pellet examinations included fuel densification and swelling measurements, fuel burnup analyses. Cladding examinations included metallography, hydrogen concentration measurement, and mechanical property testing.

3.2 Rod Design and Fabrication

Forty-two test fuel rods were manufactured, consisting of 28 full-length and 14 segmented fuel rods. The segmented rods were comprised of nine (9) individual fuel rod segments, each with its own plenum region and spring. (It is noted, that the IFPE data-base [16] does not have information about rods location in LTAs).

The standard fuel rod design consists of enriched UO_2, solid cylindrical pellets, a round wire Type 302 stainless steel compression spring, and an alumina spacer disc at each end of the fuel column. The cladding and both upper and lower end caps are composed of standard Zr-4 alloy. The rods are internally pressurized with He.

In addition to the standard design fuel rod, three additional design concepts were included in a limited number of rods in the two LTAs. These were (i) an annular fuel pellet design, (ii) large grain size pellets (35 mkm as opposed to the nominal 7 to 12 mkm standard pellet design), and (iii) cladding with graphite coating (8 mkm thickness) on the interior surface.

The main fuel rod component dimensions and rod characteristics for the full-length rods tested are shown in Table 3-1.

Table 3-1. Design Specifications for ANO-2 Full-Length Fuel Rods Used in LTAs

Parameter description	Value	
	British Units	**Metric Units***
Fuel Rod		
Overall length	161.168 in.	4093.67 mm
Diameter, Nom	0.382 in.	9.703 mm
Fuel stack length, Nom	150.0 in	3810 mm
Number of spacer disc	2	2
Spacer disc outer diameter	n/a	n/a
Spacer disc height	n/a	n/a
Plenum spring outer diameter	n/a	n/a
Plenum spring wire diameter	n/a	n/a
Plenum spring turns	n/a	n/a
Fill gas composition, Nom	He	He
Backfill gas pressure	380 psig	2.62 MPa
Rod pitch, Nom	0.506 in.	12.852 mm
Cladding		
Material type	Std Zircaloy-4	Std Zircaloy-4
Tube outer diameter, Nom	0.382 in.	9.703 mm
Tube inner diameter, Nom	0.332 in.	8.433 mm
Tube wall thickness, Nom	0.025 in.	0.635 mm
Fuel stack length, Nom	150.0 in	3810 mm
Fuel Pellets		
Material type	UO_2	UO_2
U-235 enrichment, wt.% , Nom	3.48	3.48
Pellet type, Nom	Solid / *Annular*	Solid / *Annular*
Pellet grain size, Nom (averaged)	0.394 / *0.394* mil	10 / *10* mkm
Pellet height, Nom	0.390 / *0.390* in.	9.906 / *9.906* mm
Pellet outer diameter, Nom	0.325 / *0.325* in.	8.255 / *8.255* mm
Pellet inner diameter, Nom	- / *0.092* in.	- / *2.337* mm
Initial matrix density in % T.D., Nom	95.0 / n/a	95.0 / n/a
End Chamfers & Dishes	Both Ends	Both Ends
Chamfer angle, Nom	18^0 / 18^0	18^0 / 18^0
Chamfer width and/or height, Nom	n/a / n/a	n/a / n/a
Dish depth, Nom	n/a / n/a	n/a / n/a
Dish outer diameter, Nom	n/a / n/a	n/a / n/a
Dish inner diameter, Nom	0.125 / *0.201* in.	3.175 / *5.105* mm
Pellet sintering temperature, Nom	n/a	n/a
Pellet resinter density, Nom	n/a	n/a
Pellet fabrication porosity, Nom	n/a	n/a

*British units, as the original, were converted to the metric ones.

3.3 Reactor Operational Data

The irradiation of two CE 16x16 LTAs (D039 and D040) was completed in PWR core of ANO-2. The main thermal-hydraulic parameters of the PWR core are reflected in Table 3-2.

Table 3-2. Reactor Power and Thermal Hydraulic Design Data

Parameter description	Value	
	British Units	**Metric Units***
Power and Thermal Hydraulic Parameters		
Rated Core Heat Output, Nom	2815 MWt	2815 MWt
Number Fuel Assembly in Core	177	177
Number of FR per Fuel Assembly	236	236
Heated Length, Nom	12.5 ft	381 cm
Heat generated in Fuel, Nom	0.974	0.974
Core System Pressure, Nom	2250 psia	15.513 MPa
Coolant Temperature		
Core Inlet at Power, Nom	553.5 ^{o}F	289.72 ^{o}C
Core Outlet, Nom	612.5 ^{o}F	322.50 ^{o}C
Nominal Outlet of Hot Channel	652.6 ^{o}F	344.78 ^{o}C
Coolant Flow		
Total Flow Rate at Power, Nom	120.4E6 lbm/hr	
Effective Flow Area for Heat Transfer, Nom	44.6 ft^2	4.14348 m^2
Average Velocity Along FRs, Nom	16.4 ft/s	5.0 m/s
Average Mass Flow at Power, Nom	2.605E6 lbm/ ft^2-hr	1.272E7 kg/m^2-hr

*British units, as the original, were converted to the metric ones.

3.4 Irradiation History Data

The assembly D039 was irradiated during three cycles, reactor cycles 2 through 4, for a total exposure of 885 effective full power days (EFPD). The irradiation of LTA D040 was extended through reactor cycle 6 for a total exposure of 1641 EFPD. (It is noted, that the IFPE Data-base [16] does not have information about core pattern and LTAs shuffling through the cycles).

The IFPE Data-base, distributed as FUMEX-III, V1 – 15.12.2008, presents the information about power histories for nine (9) tested rods, only. Five of them are the rods from LTA D040, which are referred as TSQ002, TSQ004, TSQ022, TSQ024 and TSQ103.

The 69 power histories for each rod include the full information about axial power distribution (25 axial nodes), fast neutron flux as well as the temperature rise along the FR estimated based on the nominal core operation conditions.

3.5 Rod Data for Assessment

The six (6) full-size rods and one (1) section rod, which were operated during 5 cycles, were used to assess the rod performances evaluation by mean the TU and PAD codes. These rods, referred as TSQ002, TSQ004, TSQ022, TSQ024, TSL095, TSL176 and TSQ103 (9 sections), were chosen based on the following:

- some of the rods were priorly characterized (cladding diameter, pellet density and volume, rod void volume);
- two pellet types, solid and annular, are utilized;
- the power histories for most examined rods are available;
- the measured rod average burn-ups cover the wide burnup range;
- the PIE data obtained for these rods covers all fuel rod performances.

The test data for the rods mentioned above are presented in Table 6-3. The additional initial data for section rod TSQ103 are shown in the same table.

The power histories of the rod TSQ002, TSQ004, TSQ022, TSQ024 and TSQ103, which are constructed based on the IFPE Data base [16], are shown in Figure A1, Appendix A.

3.6 General Assumptions Used

The following assumptions were made to obtain the unavailable data needed to simulate the fuel rod performances.

Fuel pellet and fuel rod data:

- the chamfer width and height, dish depth and dish outer diameter, which are used to calculate the adder of rod void volume, were constructed based on the solid pellet volume and density from TSQ002 data. These dimensions and the calculation of pellet dish and chamfer volume are presented in Appendix B;
- the pellet density of 95.27 %T.D. is used for TSQ004, TSQ024, TSL095 and TSL176 rods. It is noted, that in rod analysis performed by the TU code the fuel density of 95.27 %T.D. was used as a constant for all examined rods;
- the fuel fabrication porosity, which provides the fuel density of 95.27 %T.D at BOL in the TU fuel densification model, is also used by the PAD code, when the NRC fuel densification model is applied. Also, the fuel sintering temperature of 1780 ^{0}C was used, when the WEC fuel densification model is utilized;
- the plenum length for each test rod was fitted to meet the rod void volume. The void volume for TSQ004, TSL095 and TSL176 was taken as the same as for TSQ002. The void volume of TSQ022 fuel rod is applied to TSQ024 rod.

Power rod data:

- the normalized curves of axial power distribution obtained for TSQ002 rod are used for TSL095 and TSL176 rods. To obtain the rod average LHR for these rods, the multiplication coefficient given as $BU_{TSL}(EOL)/BU_{TSQ002}(EOL)$ was used. It is assumed, that this coefficient is a constant during life-time operation.

Table 3-3. Fuel Rod Data for Assessments

Rod Serial Number	Rod Void Volume, cm^3	Stack Density, %T.D.	Wokrscope for Hot Cell Examination*								
			Rod Avg. LHR , kW/ft	Rod Avg. Burnup, GWD/MTU	Local Burnup, GWD/MTU	EOL Void Vol. & Vol. Decrease at BOL, %	Cladding OD, in.	Oxide Thickness, mkm	FGR (%,) & Xe/Kr Ratio Measurement	Pellet Vol. Change, %	Pellet Den. Change, %
Full Size Rod, Solid Pellet and Std. Cladding											
TSQ002	25.42	95.27	4.692	53.24	×	×	×	×		×	×
TSQ004				50.50			×	×			
TSL095	25.91		5.046	57.26		×	×	×			
TSL176	25.32		5.047	57.27		×	×	×			
Section Rod, Solid Pellet and Std. Cladding											
TSQ103-				47.13							
#C1 (Top)	11.69	95.7		35.64		×			×		
#C2	7.79	95.7		51.16		×			×		
#C3	4.00	94.6		50.94		×			×		
#C4	3.94	94.4		50.82		×			×		
#C5	3.98	94.5		50.74		×			×		
#C6	3.96	94.4		50.76		×			×		
#C7	4.00	94.5		50.80		×			×		
#C8	3.97	94.5		48.50		×			×		
#C9(Bottom)	3.80	94.6		31.25		×			×		
Full Size Rod, Annular Pellet and Std. Cladding											
TSQ022	37.22	95.27		58.10	×	×	×	×		×	×
TSQ024				54.70			×	×			

*The data marked by "×" are presented in the following chapters.

Segmented Fuel Rod Specification

Rod ID	235-U Enrichment, %	Backfill Gas Pressure, psig (MPa)	Stack Length, inches (mm)	BOL He Volume @ STP, cm^3
TSQ103 #C1 (Top)	3.48	490 (3.378)	20.444 (519.28)	360.30
TSQ103 #C2	3.48	490 (3.378)	23.899 (607.03)	240.10
TSQ103 #C3	3.48	490 (3.378)	11.100 (281.94)	123.28
TSQ103 #C4	3.48	490 (3.378)	11.140 (282.96)	121.38
TSQ103 #C5	3.48	490 (3.378)	11.100 (281.94)	122.84
TSQ103 #C6	3.48	490 (3.378)	11.130 (282.70)	122.24
TSQ103 #C7	3.48	490 (3.378)	11.100 (281.94)	123.23
TSQ103 #C8	3.48	490 (3.378)	11.120 (282.44)	122.48
TSQ103 #C9 (Bottom)	3.48	490 (3.378)	7.160 (181.86)	117.15

4. PAD FUEL PERFORMANCE PREDICTION

4.1 Introduction

The PAD fuel rod performance prediction of the examined rods is presented in this chapter.

The base results were obtained for the nominal core operation parameters and using the PAD best estimate fuel rod models and the cladding material properties for the Standard Zircaloy-4 material. All calculations performed under this approach are referred as Case 1.

The influence of fuel swelling and densification rates on the variation of pellet density, fuel volume, rod void volume, RIP and cladding creep was also assessed. The calculations, which were carried out using the WEC fuel swelling model with the solid swelling rate constant increased by 5% from the nominal, are referred as Case 2. The calculations performed using the NRC fuel densification model with the resinter density change of - 2.75 % T.D. and - 2.25 % T.D., are referred as Cases 3 and 4, respectively.

Since the PAD code was designed for analysis of commercial full-size fuel rods, the segmented TSQ103 rod was simulated as one rod with the backfill gas pressure of 490 psig (3.378 MPa) and the fuel stack length of 118.19 inches equal to nine sections (see Table 3-3). The void volume of this rod was presented as a sum of void volumes of all sections. The initial axial power shapes of TSQ103 rod were re-built to the new fuel stack length.

4.2 Fuel Rod Burn-ups

The PAD predicted burnup versus measured burnup at EOL is shown in Figure 4-1. The local burn-ups measured for TSQ002 and the axial burnup distribution calculated are presented in Figure 4-2.

The obtained results evidence:

- the PAD data predicted are in a good agreement with the measured. The calculated rod average burnup of segmented TSQ103 fuel rod is 46.86 GWD/MTU and is close to the measured of 47.13 GWD/MTU. The inaccuracy of power distribution at the top segment C1 due to conversion of the initial axial power profiles is the main reason of the observed over-prediction (see Figure 4-1). Without this rod section, the accuracy of PAD rod average prediction is about ± 1.5 % and is within the range of the measured burnup uncertainty of +3.9/-2.6 %;
- the non-detected variation of local LHGR along the fuel stack during operation as well as the manufacturing uncertainties on the pellet density, dimensions and enrichment result in maldistribution of the burn-ups along the fuel stack. Since the data of local burn-ups were obtained based on the measurements of individual fuel pellets, the predicted PAD data is in satisfactory agreement with the experimental data. The accuracy of PAD local burnup prediction based on the presented test data lies within ± 5.0 %.

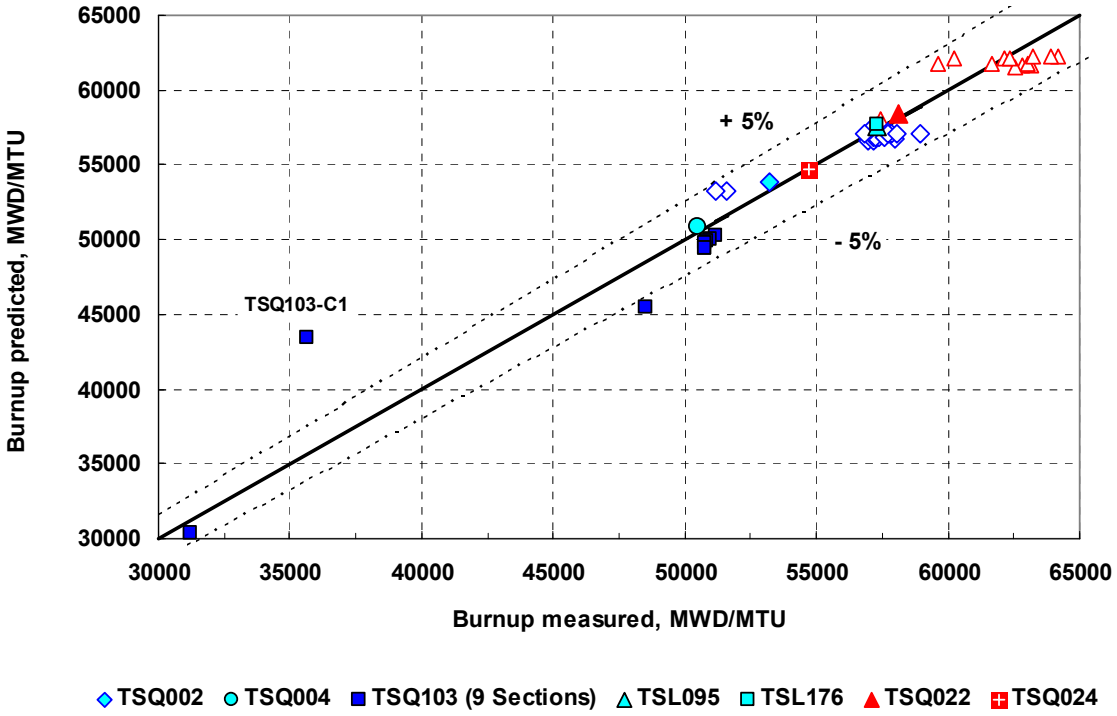

Figure 4-1. PAD predicted fuel rod burnup versus measured. (Solid symbols are the rod average burn-ups; open symbols are the local burn-ups).

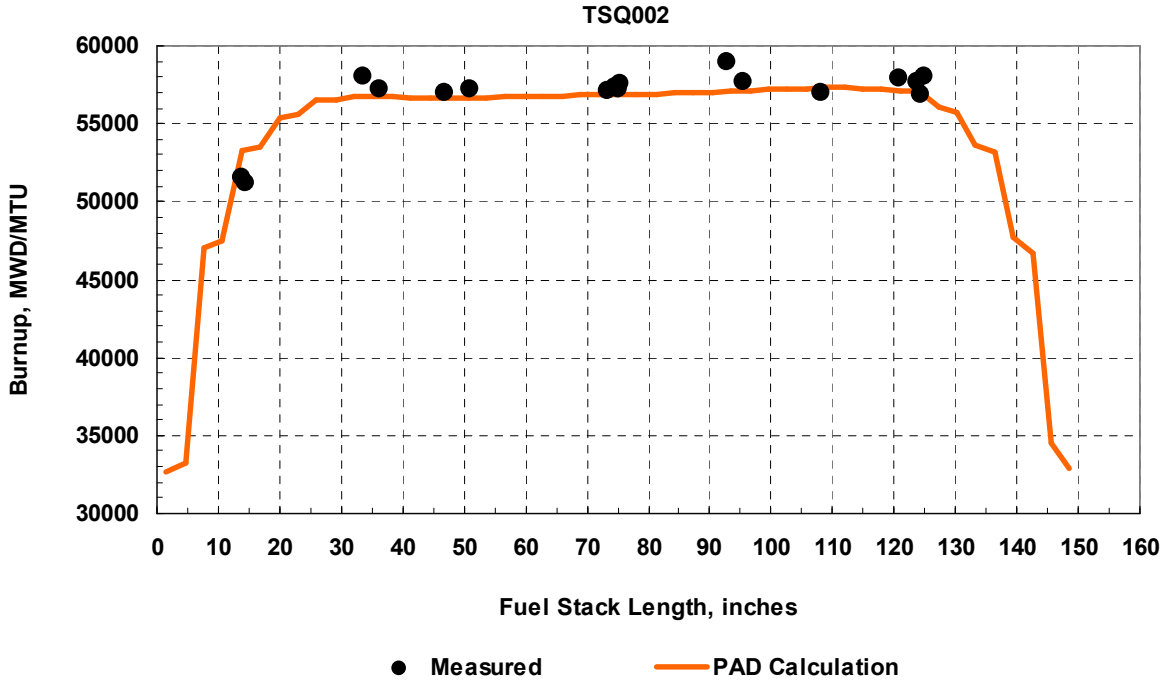

Figure 4-2. Measured and PAD predicted fuel rod burnup variation for TSQ002 fuel rod.

4.3 Cladding Corrosion

The variation of the peak oxide thickness versus rod time-average LHR obtained for the examined fuel rods and data predicted by PAD is presented in Table 4.-1

Table 4-1. Measured and PAD Predicted Peak Oxide Thickness

Rod ID	Data measured		PAD code data predicted	
	Rod Time-Avg. LHR, kW/ft (kW/m)	Peak Oxide Thickness, mkm	Rod Time-Avg. LHR, kW/ft (kW/m)	Peak Oxide Thickness, mkm
TSQ002	4.692 (15.39)	53	4.685 (15.37)	54
TSQ004	-	-	4.427 (14.52)	44
TSL076*	5.076 (16.65)	61	-	-
TSL095	5.046 (16.56)	59	5.011 (16.44)	64
TSL176	5.047 (16.56)	64	5.022 (16.48)	65
TSQ022	4.735 (15.53)	43	4.756 (15.60)	56
TSQ024	-	37	4.476 (14.69)	49

* The data for this rod were taken from the PIE data-base [16] and is used for comparison only.

The table shows:

- in general, the PAD data predicted are in satisfactory agreement with the measured;
- the PAD code predicts the growth of oxide thickness, when the rod time-average LHR increases. At the same time, as can be seen, this dependence for the measured data is not well-defined.

There are some reasons which can impact the cladding oxide thickness variation at the same operation parameters: coolant inlet temperature, core mass flow rate and LHR. Some of these reasons are (i) the crud deposited on the cladding and (ii) the rod "hot-channel" hydraulic diameter (D_e) variation. The first one, due to the higher thermal conductivity, will increase the oxide thickness during operation. The increase in D_e due to manufacturing uncertainties on the rod pitch and the cladding outer diameter as well as irradiation-induced relaxation of the cell springs supporting the rods will decrease the coolant temperature rise.

The sensitivity analysis was performed for two pre-characterized FRs – TSQ002 and TSQ022. The crud layer was varied in the range of 2.5 – 7.5 mkm (0.1 ÷ 0.3 mils), the value D_e was taken as 5% over the nominal value of 11.9736 mm (0.4714 inches).

Influences of the crud thickness and the hydraulic diameter change on oxide thickness variation for TSQ002 fuel rod are displayed in Figure 4-3. The measured axial variation of oxide thickness for TSQ022 fuel rod and PAD data predicted for the different values D_e used are shown in Figure 4-4. The presented results demonstrate:

- the PAD code well predicts the oxide thickness variation along the fuel stack;
- a small increase in D_e by ~0.6 mm decreases the peak oxide thickness by ~6 mkm.

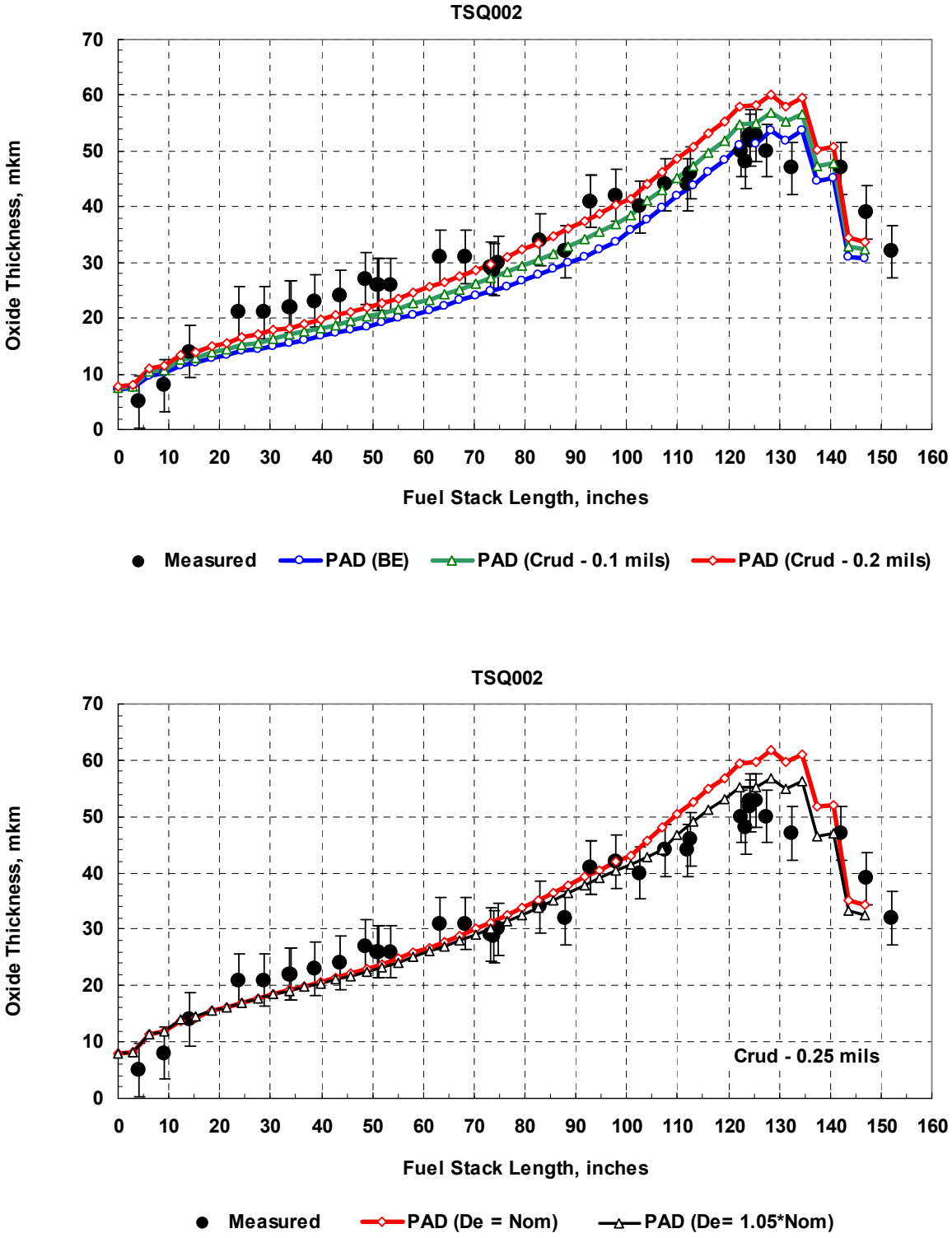

Figure 4-3. Measured and PAD predicted axial oxide thickness variation for TSQ002 fuel rod.

(It is noted, that the presented oxide thickness data were made by ECT corrected based on correction between ECT and metallographic measurements. Using the conversion equation and the direct metallographic data the accuracy on the determination of the oxide thickness was ~4 mkm for 1σ confidence level).

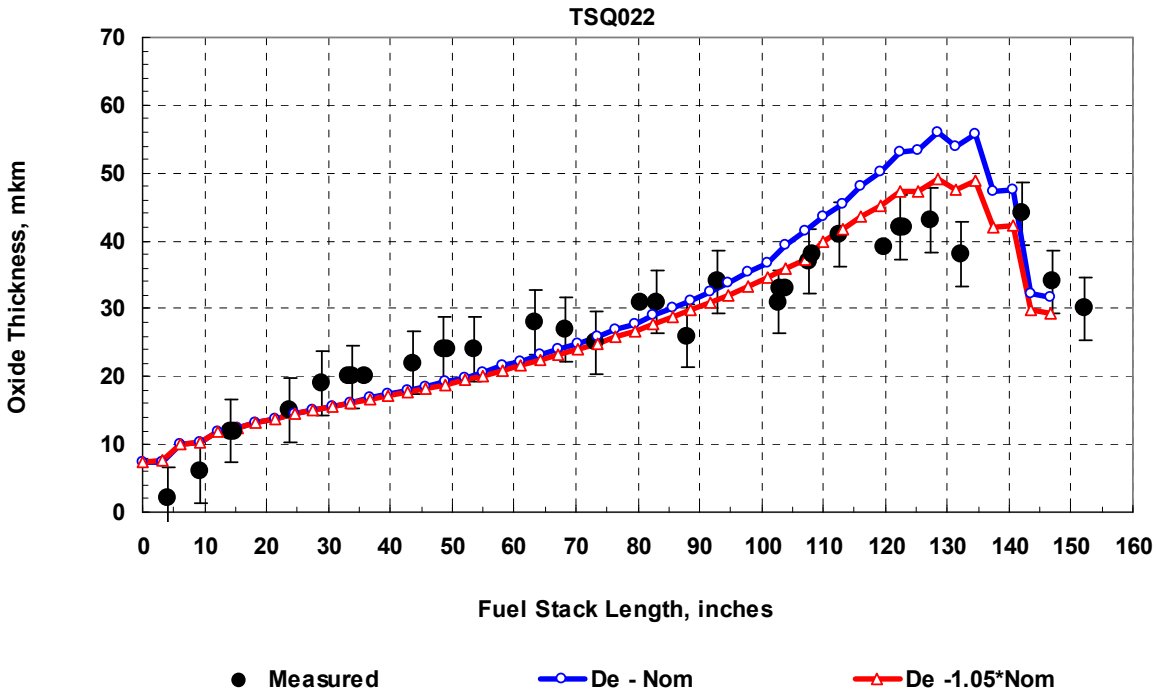

Figure 4-4. Measured and PAD predicted axial oxide thickness variation for TSQ022 fuel rod.

4.4 Fuel Densification and Swelling

The measured and PAD predicted data of the fuel density change under irradiation for both solid and annular pellets are presented in Figure 4-5. The WEC and the NRC fuel densification and swelling models were used for assessment. The obtained results evidence:

- within the measured uncertainties the WEC model predicts well the fuel density change for both solid pellet types (Cases 1 and 2). The increase in solid fission product swelling rate constant provides a better agreement based on the average data (Case 2);
- within the measured uncertainties the PAD data calculated using the NRC model (Cases 3 and 4) is in satisfactory agreement with the experimental data obtained for the solid pellets. As burnup grows, the prediction data based on the fuel resinter density change of -2.25 begins to be overestimated (Case 4). For annular pellets the NRC model with fuel resinter density change of (-2.75 ÷-2.25) overestimates the fuel density by ~ 0.5 %.

The measured and the PAD predicted data of the fuel volume change, ΔV/V, versus burnup are displayed in Figure 4-6. Since the number of experimental data is limited, in order to obtain the trend of the curve of fuel swelling the calculations were performed in the wide burnup range using different PAD fuel swelling and densification models. These data are presented in the same figure.

The calculated data of fuel swelling agree well with the fuel density change results. Based on the calculation results the average and the bounding curves of fuel swelling were built (see Figure 5-6, dashed curves). The presented data demonstrate:

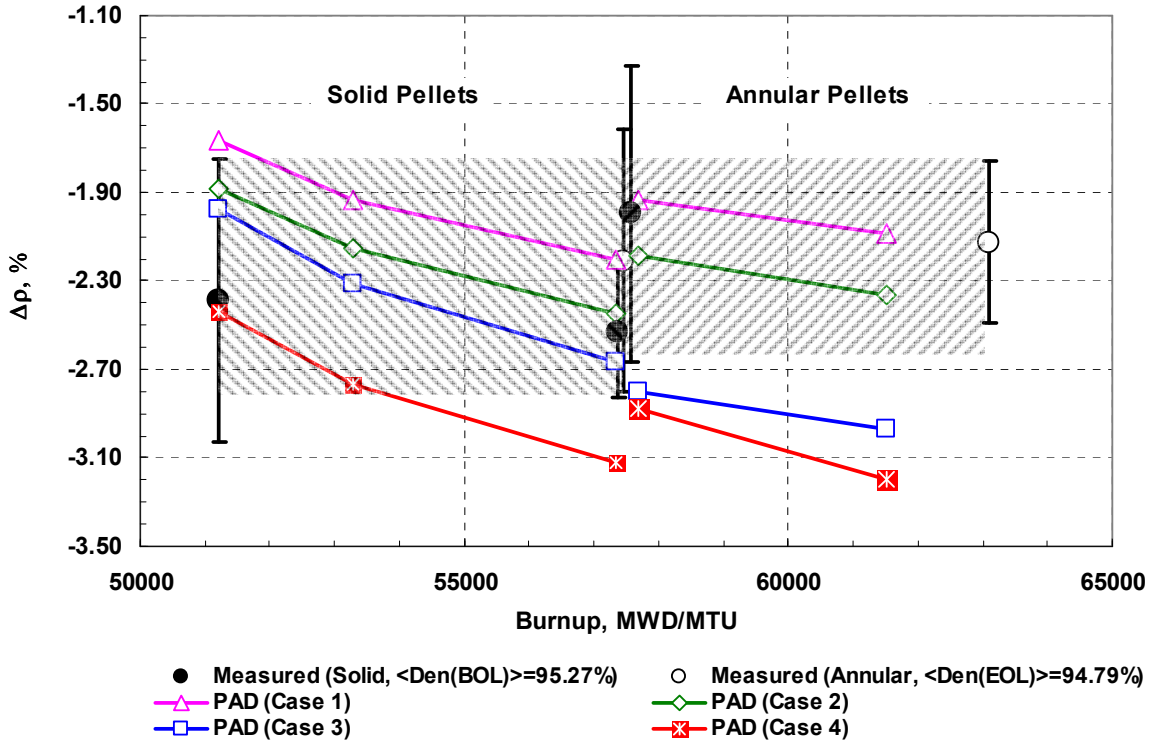

Figure 4-5. Measured and PAD predicted fuel pellet density change versus burnup. (The density change, Δρ, is determined as ρ_{EOL}(%T.D.) - ρ_{BOL}(%T.D.))
(It is noted, that the uncertainty on the determination of pellet density was determined for each examined pellet based on the measurement data presented in the PIE Report and taken at 1σ confidence level).

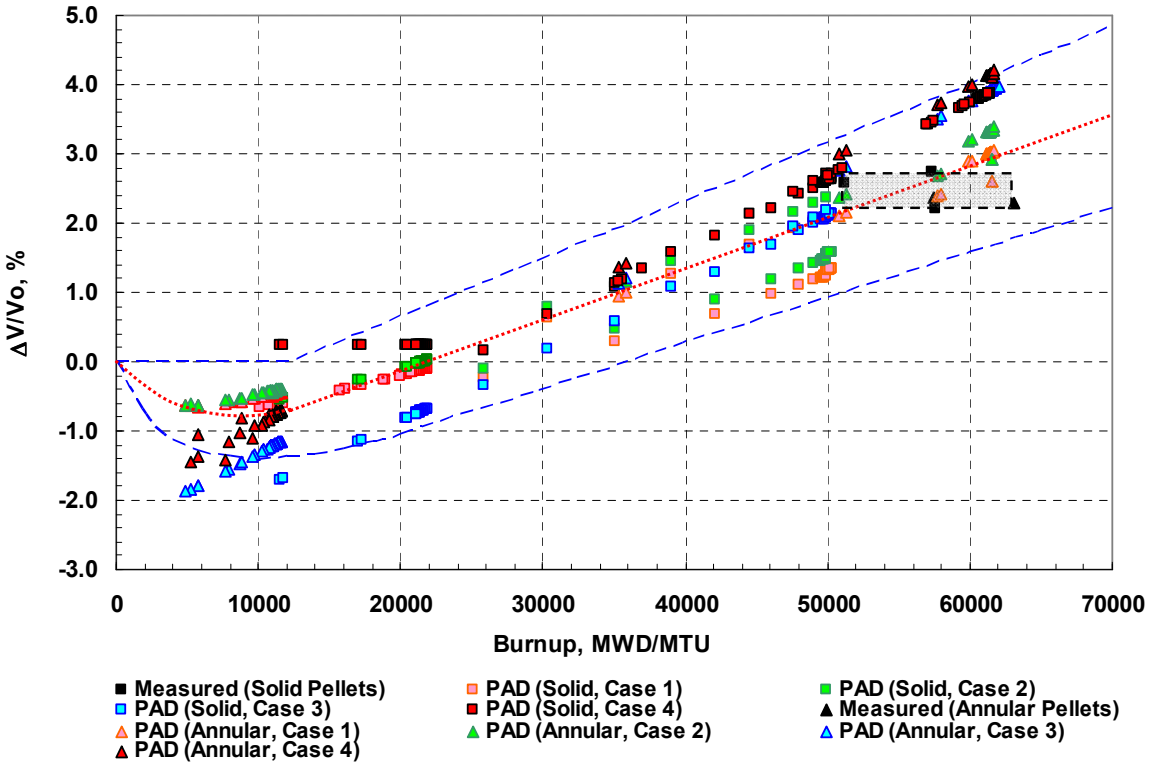

Figure 4-6. Measured and PAD predicted fuel swelling versus burnup.

- both the PAD fuel swelling and densification models provide the acceptable agreement with the measured data;
- the use NRC densification model with the small value of fuel resinter density change provides the upper bound of fuel swelling. In the case, when the value of fuel resinter density change is less than -2.25, the lower bound of fuel swelling is reached;
- the WEC model based on the BE fuel swelling and densification rates provides better agreement with the experimental results on the basis of the averaged data for solid and annular pellets in the burnup range of 50-63 GWD/MTU.

The calculation results of fuel swelling obtained by the PAD code on the basis of TSQ fuel rods operated in ANO-2 core are in satisfactory agreement with the experimental data obtained for fuel rods operated in the cores of others power plants: PWRs, BR-3 [42] and VVER [43]. These data are presented in Figure 4-7. It is noted, that the PAD data for VVER fuel (annular pellets) were calculated for the FR nominal dimensions and with fuel density of 94.89 % T.D. (10.4 g/cm^3) [16].

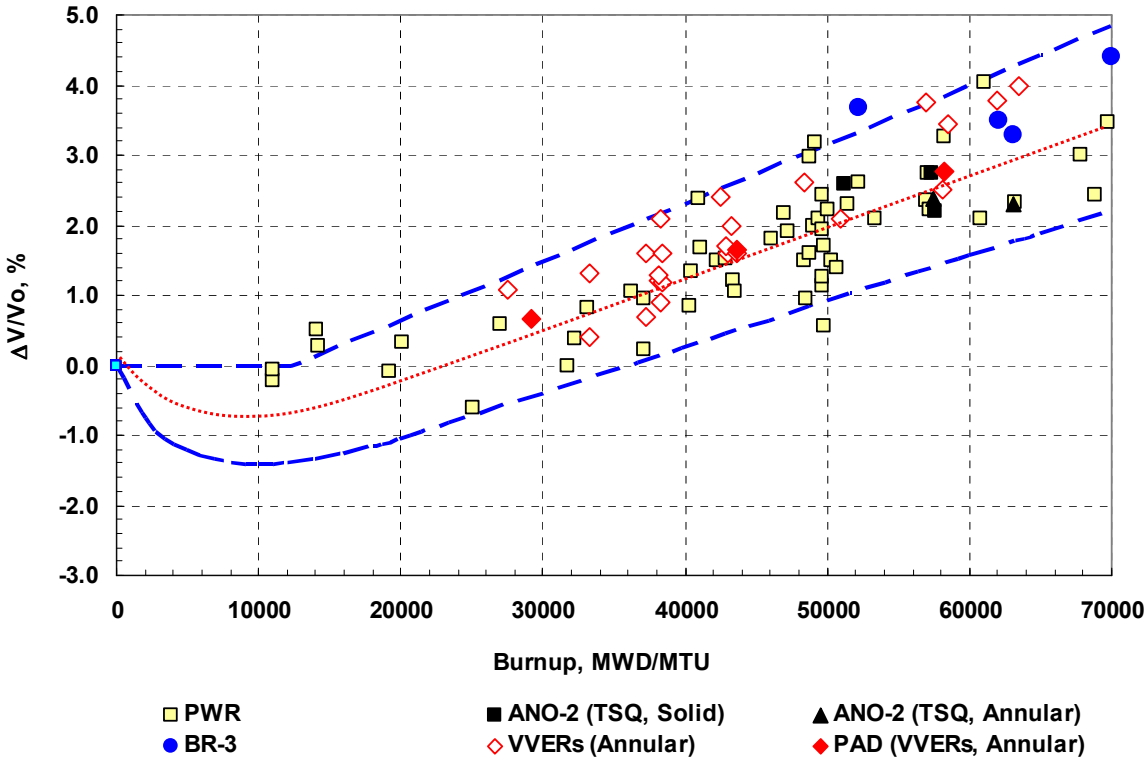

Figure 4-7. Measured and PAD predicted fuel swelling of fuel rods operated in different cores of PWR, VVER (1000 & 440) and BR3 reactor.

4.5 Cladding Creep

The cladding strain is the integral effect of cladding thermal and irradiation creep, cladding growth and fuel swelling. The PAD cladding strain predicted for the examined rods and the measured data are collected in Table 4-2.

Table 4-2. Measured and PAD Predicted Cladding Strain.

Rod ID	Cladding strain measured, % (averaged in the range from ~20 in. (from the bottom of fuel stack) to 150 in.)	PAD cladding strain predicted, % (averaged in the range from ~20 in. (from the bottom of fuel stack) to 150 in.)
TSQ002	- 0.65	- 1.11
TSQ004	- 0.64	- 1.00
TSL076*	- 1.06	-
TSL095	- 0.92	- 1.09
TSL176	- 0.91	- 1.09
TSQ022	- 0.58	- 1.05
TSQ024	- 0.73	- 1.04

* The data for this rod were taken from the PIE data-base [16] and is used for comparison only

The table shows that the predicted cladding strain based on the PAD BE fuel rod model parameters (WEC fuel swelling and densification; cladding irradiation creep):

- is slightly overestimated for the pre-characterized fuel rods (TSQ_002/004/022/024);
- is in satisfactory agreement with the measured for the fuel rods manufactured with the design dimensions on the cladding.

Since the data of cladding outer diameter change along the fuel stack are original, the comparative analysis for the pre-characterized FRs (TSQ_002/022) and for the fuel rods manufactured with design dimensions (TSL_095/176) was made. The WEC and NRC fuel swelling and densification models were used for this analysis. The measured and the predicted cladding outer diameter change for the examined fuel rods are presented in Figures 4-8 through 4-10.

The figures demonstrate:

- the predicted data for TSL_095 & 176 rods based on the PAD BE fuel rod models agree well with the measured. The decrease in cladding irradiation creep by 15% from the nominal as well as the increase in the fuel swelling rate constant in the WEC model (Case 2) envelopes the experimental data with account for the oxide thickness measurement uncertainty and pellet density variation (94.6 – 95.5 % T.D.);
- the use of PAD NRC fuel swelling model with the minimal fuel resinter density change (Case 4) bounds the measured data of all examined FRs with different pellet types and with account for the variation of pellet density, cladding geometrical dimensions as well as for the measurement uncertainties on the cladding outer diameter an oxide thickness.

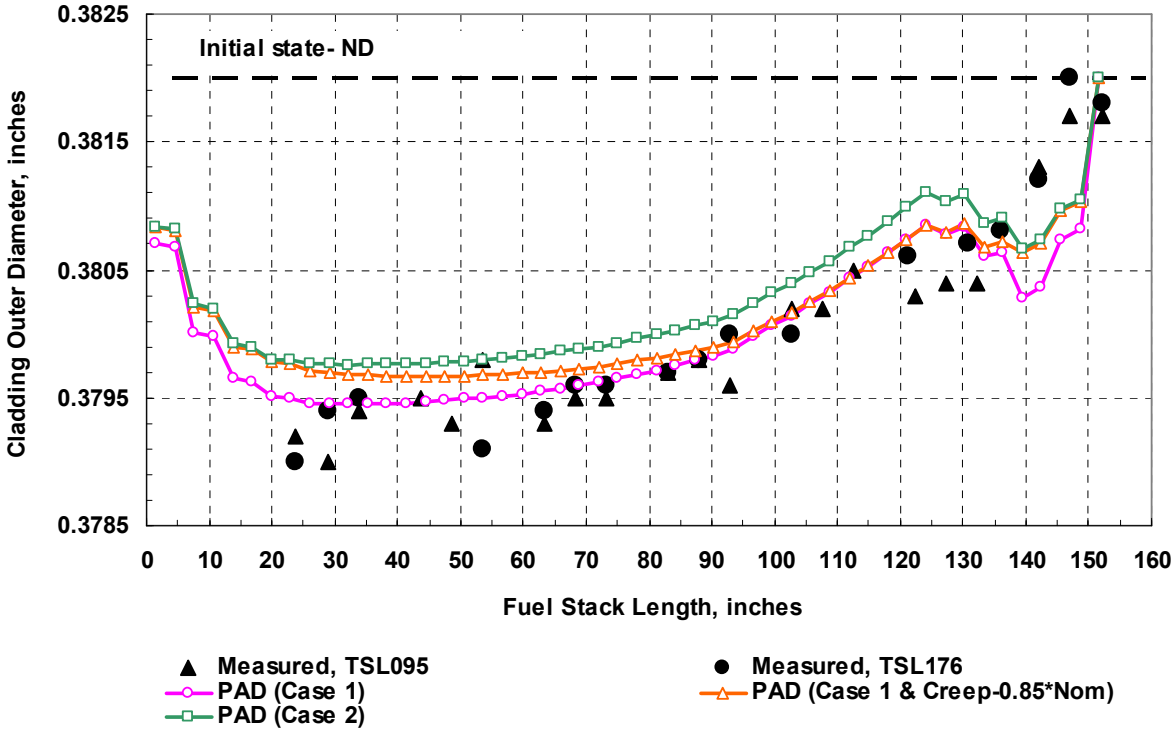

Figure 4-8. EOL measured and PAD predicted cladding outer diameter change for TSL_095/176 fuel rods.

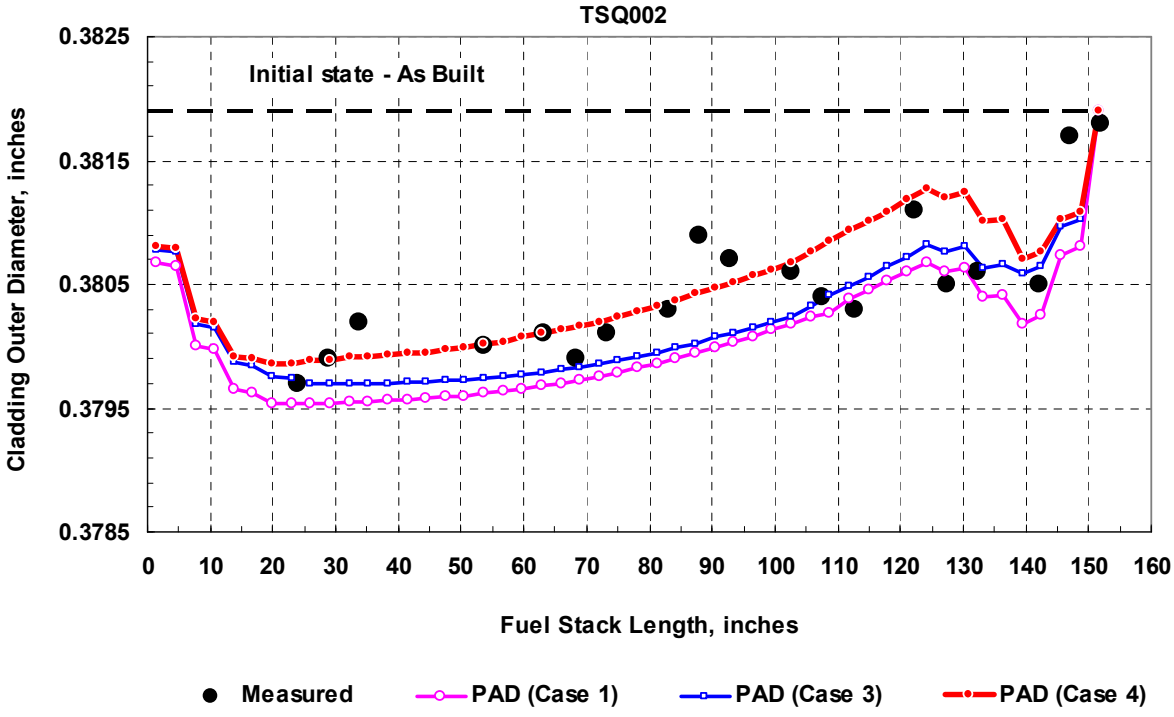

Figure 4-9. EOL measured and PAD predicted cladding outer diameter change for TSQ002 fuel rod.

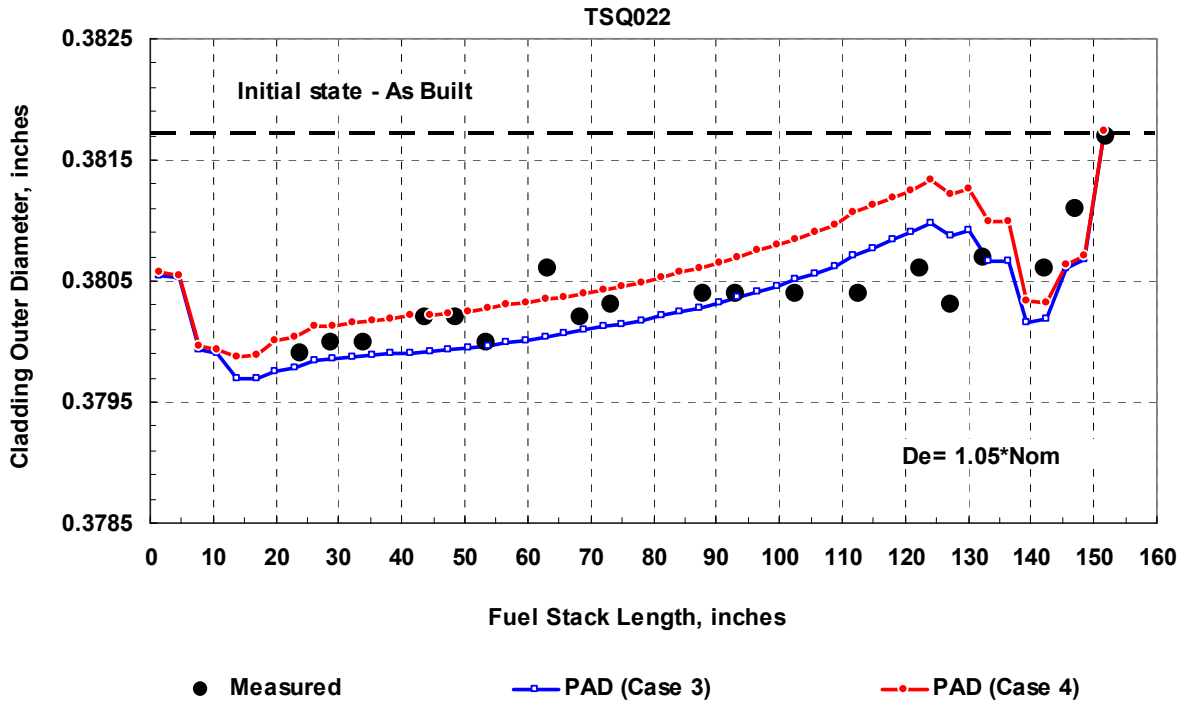

Figure 4-10. EOL measured and PAD predicted cladding outer diameter change for TSQ022 fuel rod.

4.6 Fuel Rod Growth

As published in the report [44], the irradiation growth of LTA D040 fuel rods was in the range of (0.83 – 1.10) %. The PAD calculations for the examined fuel rods show increase in FR irradiation growth from 0.88% to 0.95%. Thus, the predicted values based on the BE FR model growth are within the measured one.

Using the upper bound fast neutron flux conversion coefficients in the PAD 16×16 core model, the FR irradiation growth increases from 0.95 % to 1.03 % and is close to the measured one.

4.7 Fuel Rod Void Volume

The FR void volume change ($\Delta V_V/V_0$) is very sensitive to the fuel fabrication porosity, pellet geometry, fuel rod component dimensions and depends on the fuel densification and swelling, the value of cladding creep-down and rod growth.

The measured and the PAD predicted FR void volume change based on the ND and BE fuel rod models are collected in Table 4-3.

Table 4-3. Measured and PAD Predicted Fuel Rod Void Volume Change.

Rod ID	Measured data		PAD predicted data	
	Initial Void Volume, V_0, cm^3	EOL $\Delta V_V / V_0$, %	Initial Void Volume, V_0, cm^3 (in^3)	EOL $\Delta V_V / V_0$, %
TSQ002	25.42	-30.0	25.42 (1.5512)	-24.9
TSQ004	-	-	25.42 (1.5512)	-22.3
TSL076*	26.12	-26.9	-	-
TSL095	25.91	-29.0	25.91 (1.5811)	-26.0
TSL176	25.32	-27.7	25.32 (1.5451)	-26.6
TSQ022	37.22	-16.7	37.22 (2.2715)	-18.3
TSQ024	-	-	37.22 (2.2715)	-17.2

* The data for this rod were taken from the PIE data-base [16] and is used for comparison only

The table shows:

- the predicted data for the FRs with solid pellets are underestimated by 5%, as a maximum;
- for the fuel rods with the annular pellets, the predicted void volume change is slightly overestimated by 1%.

The influence of fuel swelling on the void volume change was assessed for the examined rods with both pellet types. The calculation used the NRC fuel densification model (Cases 3 and 4). The obtained results, as was expected, showed that decrease in fuel resinter density change leads to decrease in the difference between the predicted and measured data for the rod with solid pellets and provides the opposite effect for FR with annular pellets.

It should be noted, that the PAD void volume model takes into account all rod components void volumes (see Chapter 2.1). The fitting of this volume to the measured one can bring uncontrolled mistakes. Thus, the well described fuel rod component dimensions will provide more productive results.

4.8 Fission Gas Release and Rod Internal Pressure

The EOL measured and the PAD predicted fission gas release for the examined fuel rods are presented in Figure 4-11. The figure demonstrates:

- the calculated data based on the BE model of fission gas release for the steady-state operation are overestimated. The difference at the average rod burnup of about 30 GWD/MTU is ~ 0.1 % and ~ 0.36 % on the average basis at BU ~ 50 GWD/MTU;
- the FGR of 1.5 % is predicted by PAD for the tested rod with the high burnup of ~ 58 GWD/MTU.

The rod void volume and gas volume measured at EOL were used to obtain the RIP. These data and the PAD predicted RIP values for the examined FRs are presented in Figure 4-12.

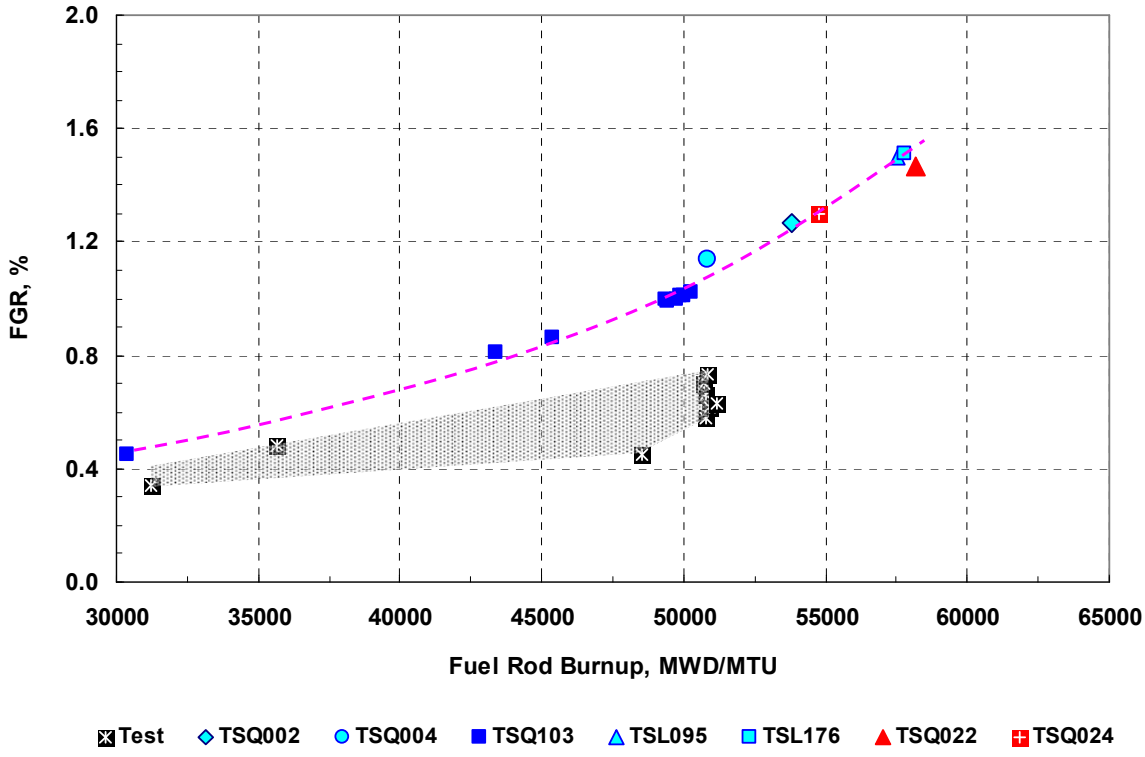

Figure 4-11. EOL measured and PAD predicted fission gas release.

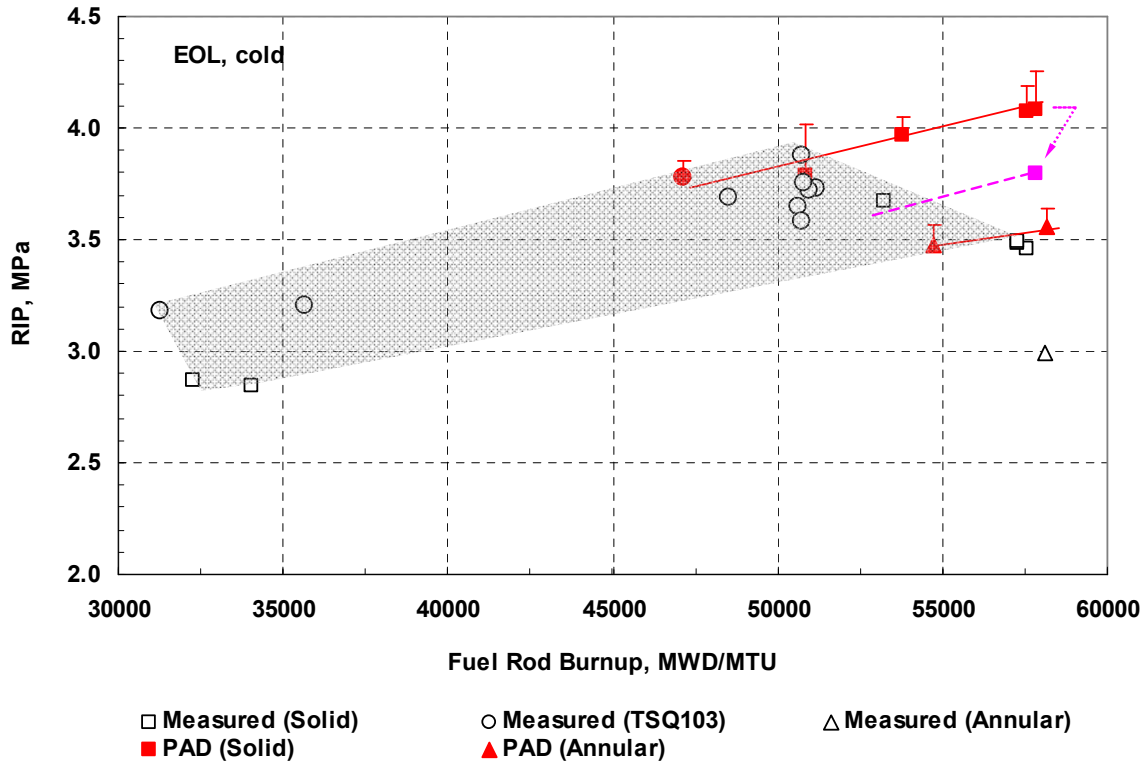

Figure 4-12. EOL measured and PAD predicted rod internal pressure.
(The arrow shows the RIP change, when the UB FR model growth is used only).

The data presented in Figure 4-12 show:

- the calculated RIP is higher for FRs with solid pellets in comparison with FRs with annular pellets. This difference reaches ~ 0.5 MPa at the rod burnup of ~ 57 GWD/MTU;
- the predicted RIP based on the BE FR model parameters is overestimated. The difference reaches 0.5 MPa at the high burnup of ~ 58 GWD/MTU.

The rod internal pressure depends directly on the rod void volume. Any uncertainties related with FR design parameters (variation of initial backfill gas pressure, rod component dimensions and etc.) or deviation from the nominal code FR model parameters can significantly impact the RIP value. The sensitivity analysis was performed using the UB FR model growth (see Figure 4-12). The obtained result demonstrates decrease in the difference between the predicted and measured data.

4.9 Conclusion

The PAD cod ability to predict the fuel performances was demonstrated based on the IFPE database of the OECD/NEA. The experimental data obtained for the 16×16 LTA D040 fuel rods operated at steady-state in ANO-2 PWR core during five cycles up to rod average burnup of ~ 60 GWD/MTU have been utilized.

The rod average and local burn-ups, the cladding corrosion, the cladding creep (rod outer diameter change at EOL), the rod irradiation growth, the fuel densification and swelling, the fuel void volume, the fission gas release and rod internal pressure at EOL, cold were calculated based on the PAD best estimate fuel rod models. Two different fuel densification and swelling models, WEC and NRC, were used to assess the model parameters.

The fuel performance predictions made by the PAD code are in satisfactory agreement with the experimental data obtained for the examined fuel rods with solid and annular pellets. The PAD fuel densification and swelling models describe well the fuel volume change for the fuel rods operated in PWRs and VVER cores up to high burn-up.

5. TRANSURANUS FUEL PERFORMANCE PREDICTION

5.1 Introduction

The TRANSUARNUS fuel rod performance prediction for the examined LTA D040 fuel rods is presented in this chapter. The calculation used the TU code version of v1m1j06.

The calculations have been carried out coherently with the power histories and operation conditions and using the specifications and pre-irradiation characterization data of the analyzed rods (see Chapter 3).

The TU fuel rod models, which take into account the relevant phenomena occurring in the fuel and the specific features of PWR type rod, were used in the present analysis. These models are presented in Table A1, Appendix A ("reference setting"). The value of fuel pore removable during sintering of 1.54% and burnup at which sintering has stopped of 5 GWD/MTU were used as the BE basis. The TU calculation results, which are obtained based on the above parameters, are referred as Case 1.

A sensitivity study has been performed starting from the "reference setting" and testing some TU fuel densification and swelling model parameters:

- the axial anisotropy factor for fuel densification (*beta* = 0.1). The data calculated using this setting is referred as Case 2;
- the fuel pore removable value of 2.34% with burnup of 12 GWD/MTU. The data obtained using this setting is referred as Case 3.

5.2 Fuel Rod Burn-ups

The TU computed burn-ups versus measured at EOL are shown in Figure 5-1. The figure demonstrates:

- the calculated TU burn-ups are slightly underestimated, and this effect is observed in the wide range of (40 ÷ 60) GWD/MTU;
- for the fuel rod average burnup the underestimation is 2.7% on the average with standard deviation of 3.5%;
- for the local burnup, the TU is underestimated by 5.3% on the average with standard deviation of 1.7%.

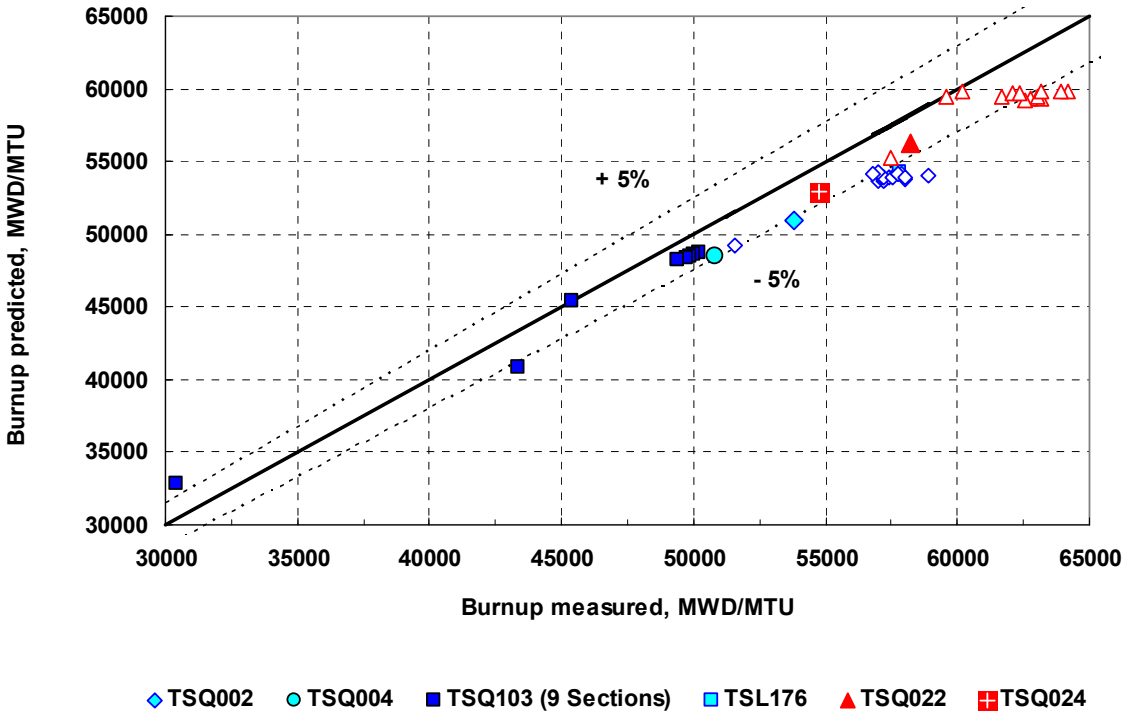

Figure 5-1. TU predicted fuel rod burnup versus measured. (Solid symbols are the rod average burn-ups; open symbols are the local burn-ups).

5.3 Cladding Corrosion

The variation of the peak oxide thickness versus rod time-average LHR for the examined fuel rods and data predicted by the TU code is presented in Table 5.-1

Table 5-1. Measured and TU Predicted Peak Oxide Thickness

Rod ID	Data measured		TU code data predicted	
	Rod Time-Avg. LHR, kW/ft (kW/m)	Peak Oxide Thickness, mkm	Rod Time-Avg. LHR, kW/ft (kW/m)	Peak Oxide Thickness, mkm
TSQ002	4.692 (15.39)	53	4.685 (15.37)	20.6
TSQ004	-	-	4.427 (14.52)	19.2
TSL176	5.047 (16.56)	64	5.022 (16.48)	22.9
TSQ022	4.735 (15.53)	43	4.756 (15.60)	21.3
TSQ024	-	37	4.476 (14.69)	19.6

The table shows:

- the computed data of cladding oxide thickness are underestimated for all tested FRs;

- the increase in LHR from 14.5 kW/m to 15.6 kW/m does not significantly impact on cladding corrosion;
- the increase in fast neutron fluence or rod burn-ups from ~51 GWD/MTU (TU_TSQ002) to ~56 GWD/MTU (TU_TSQ022) leads to growth in the peak oxide thickness by 0.7 mkm, only.

5.4 Fuel Densification and Swelling

The measured and TU predicted data of the fuel density change under irradiation for both solid and annular pellets are presented in Figure 5-2. The different fuel densification parameters were used for assessment. The obtained results evidence:

- within the measured uncertainties the use of fuel densification parameters of *denpor* = 0.02 and *denbup* = 5 GWD/MTU predicts well the fuel density change for both solid pellet types up to burnup of ~60 GWD/MTU and overestimates, when the fuel burnup grows up to ~65 GWD/MTU (Cases 1);
- the increase in the percentage of fuel porosity removable at the end of sintering with the burnup value of 12 GWD/MTU leads to underestimation of the fuel density change by ~1% on the average at burnup of 51 GWD/MTU and provides a satisfactory agreement with the measured data obtained for the solid and annular pellets with burnup of 57 GWD/MTU and higher (Case 3).

The measured and the TU predicted data of the pellet volume change are displayed in Figure 5-3. To obtain the trend of the curve of fuel swelling, the calculations were performed in the wide burnup range; these data are shown in the same figure. The presented data correlate with the previous results of pellet density change and demonstrate:

- the TU fuel swelling and densification model with parameters *denpor* = 0.02 and *denbup* = 5 GWD/MTU (Case 1) provides acceptable agreement with the measured data in the burnup range of 50÷55 GWD/MTU and overestimates, when the BU > 55 GWD/MTU. The comparison with the data obtained during PAD analysis shows that the used fuel densification parameters increase the pellet volume at burnup of 10 ÷20 GWD/MTU and it is the UB for the most PWR fuel rods;
- the increase in the fuel densification factor (*denpor* = 0.012, *denbup* = 12 GWD/MTU, Case 3) leads to underestimation of the fuel volume change at BU ~ 50 GWD/MTU and provides good correlation with the measured data for both fuel pellet types in the high burnup region. The comparison with the data obtained during PAD analysis demonstrates that the used fuel densification parameters provide better agreement with the BE data for PWR fuel rods.

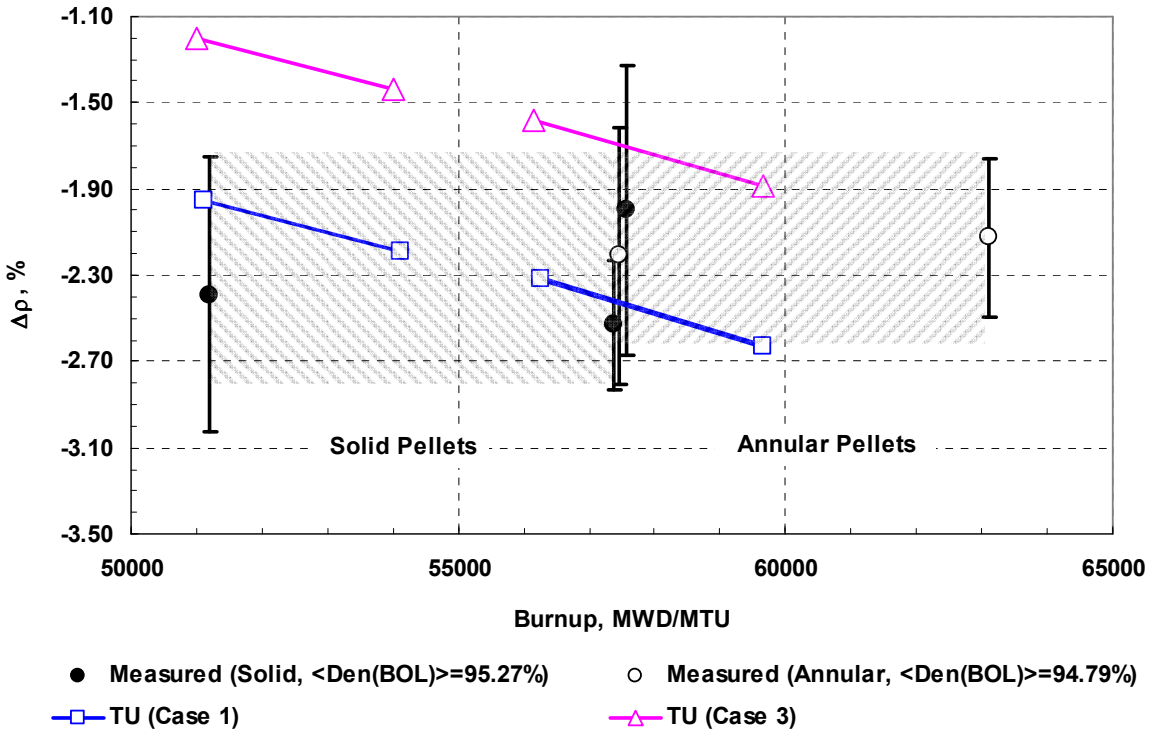

Figure 5-2. Measured and TU predicted fuel pellet density change versus burnup. (The density change, Δρ, is determined as ρ_{EOL}(%T.D.) - ρ_{BOL}(%T.D.))

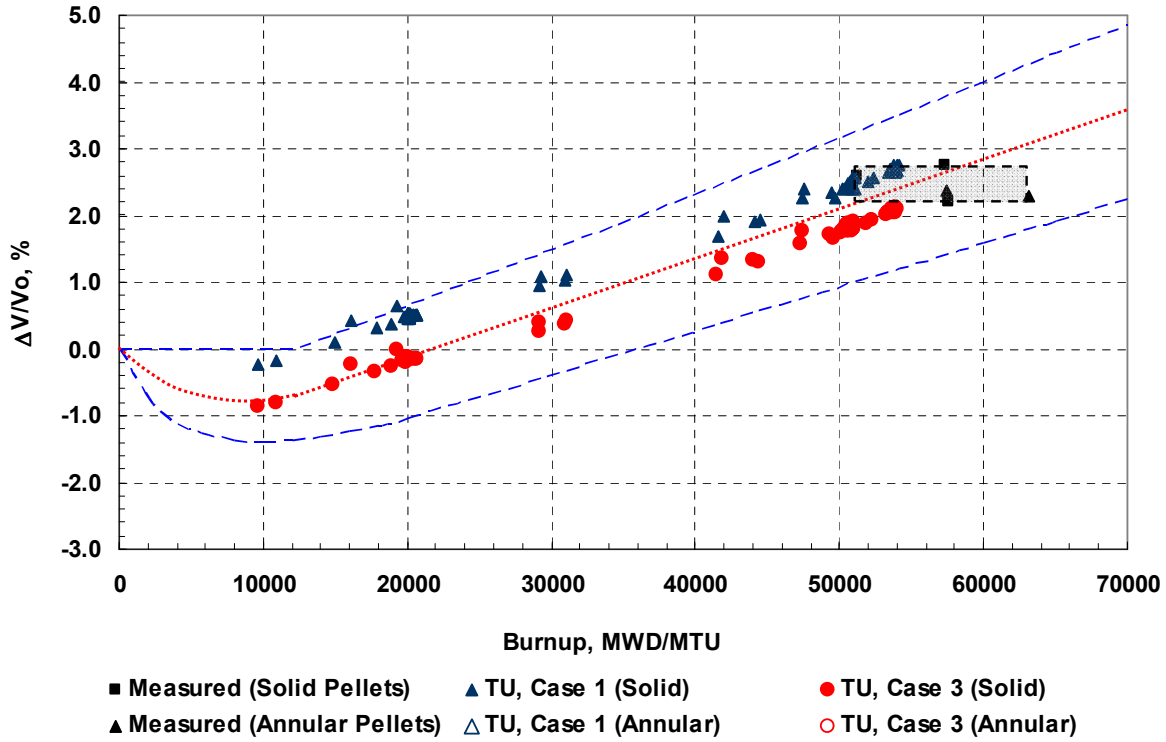

Figure 5-3. Measured and TU predicted fuel swelling versus burnup.
(The dashed lines represent the UB, BE and LB of fuel volume change from Figure 4-6)

5.5 Cladding Creep

The measured and the TU predicted cladding strain data for the examined fuel rods are presented in Table 5-2. The calculations were performed for different TU model parameters to assess the effect of fuel swelling and densification.

Table 5-2. Measured and TU Predicted Cladding Strain.

Rod ID	Cladding strain measured, %	TU cladding permanent tangential strain, % (averaged along the fuel stack)		
		Case 1	Case 2	Case 3
TSQ002	- 0.65	- 0.56	- 0.69	- 0.77
TSQ004	- 0.64	- 0.64	- 0.77	- 0.85
TSL076*	- 1.06	-	-	-
TSL095*	- 0.92	-	-	-
TSL176	- 0.91	- 0.42	- 0.56	- 0.64
TSQ022	- 0.58	- 0.59	- 0.67	- 0.76
TSQ024	- 0.73	- 0.50	- 0.63	- 0.70

***** The data for these rods were taken from the PIE data-base [16] and are used for comparison only.

The table allows to conclude:

- the cladding strain calculated on the BE basis (Case 1) is slightly underestimated by ~ 0.1 % on the average for the pre-characterized fuel rods (TSQ_002/004/022/024). However, for the fuel rods of TSL serial number the underestimation is twofold;
- in general, the difference between the measured and predicted data decreases, when the axial anisotropy factor for densification (Case 2) was taken into account, or due to the increase in fuel pellet densification factor (Case 3).

The conclusions made above are supported by the data of cladding outer diameter change at EOL, cold. The measured and the TU predicted cladding outer diameter change along the fuel stack for the fuel rods with solid and annular pellets are presented in Figures 5-4 and 5-5, respectively.

The figures demonstrate:

- the predicted data based on the BE basis (Case 1) are overestimated for all examined fuel rods;
- the data obtained using both the axial anisotropy factor for densification (*beta* = 0.1, Case 2) and the densification parameters of *denpor* = 0.12 and *denbup* = 12 GWD/MTU (Case 3) are in satisfactory agreement with the measured ones with accounting for the underestimation of the cladding oxide thickness value.

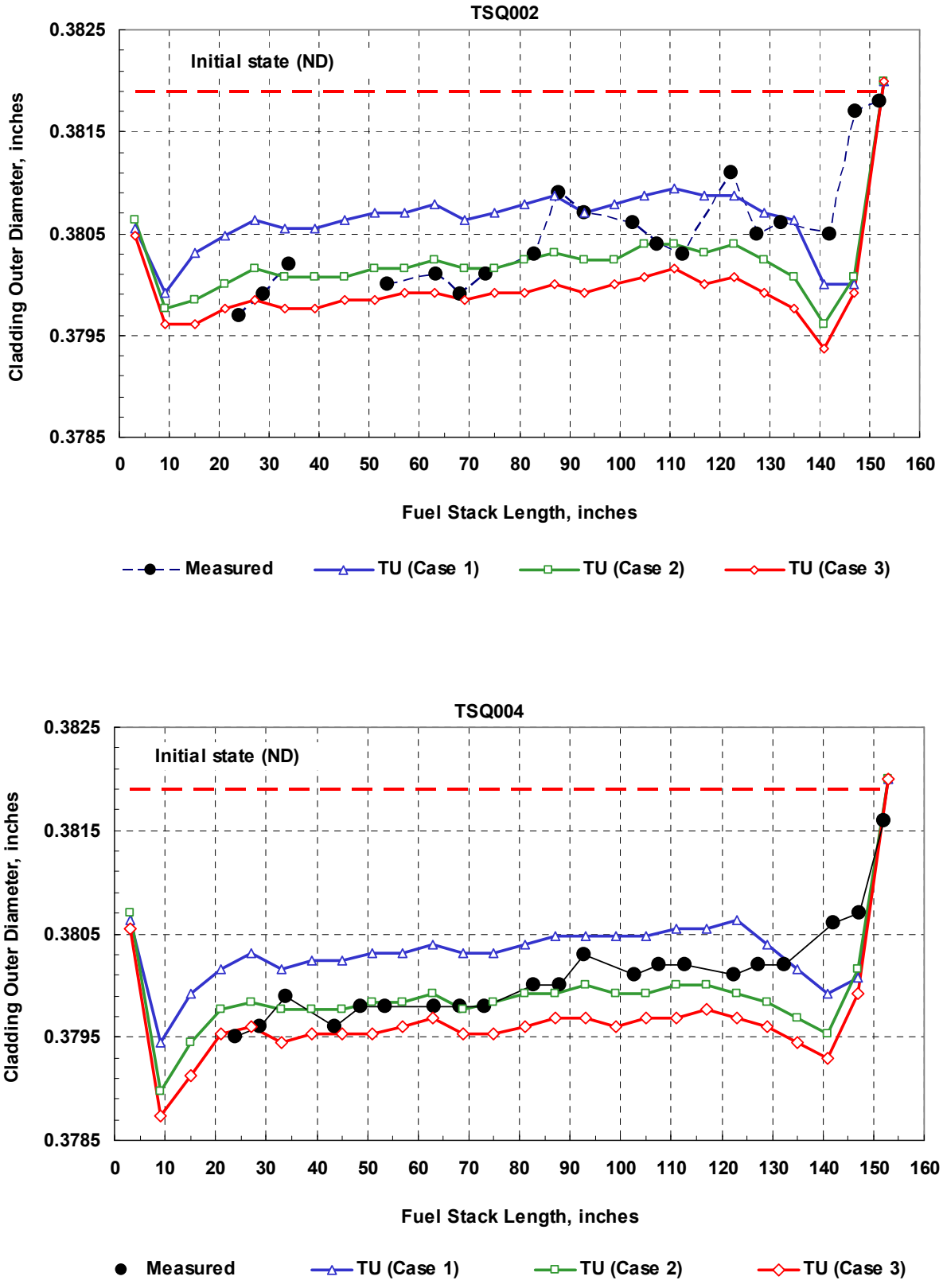

Figure 5-4. Measured and TU predicted cladding outer diameter change at EOL cold for the fuel rods with solid pellets.

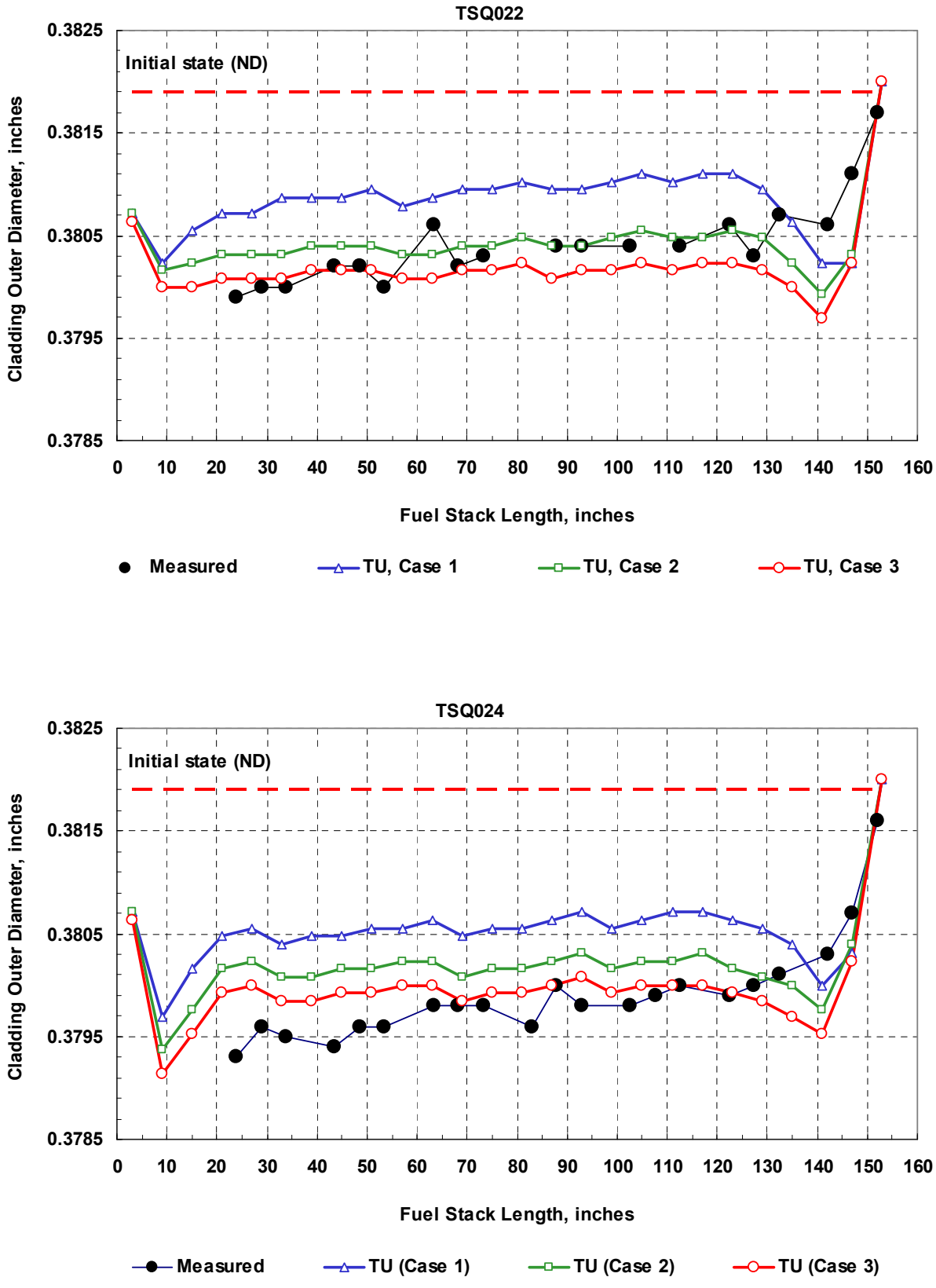

Figure 5-5. Measured and TU predicted cladding outer diameter change at EOL cold for the fuel rods with annular pellets.

5.6 Fuel Rod Growth

The measured [44] and the TU predicted data of fuel rod growth are collected in Table 5-3. The presented data show:

- with increased burnup the predicted data calculated on the BE basis (Case 1) are ~1.05% on the average, which is at the upper boundary of the measured ones. The additional calculations performed without static and sliding frictions between the fuel pellets and the cladding do not significantly impact on FR growth;
- the change in fuel densification and swelling model parameters, which provide the satisfaction agreement with the other measured FR performances, causes increase in FR growth by 0.06% on the average (see Cases 2 and 3).

Table 5-3. Measured and TU Predicted Fuel Rod Growth.

Measured Data		Rod ID	TU Predicted Data			
Avg. BU, GWD/MTU	FR Growth, %		Avg. BU, GWD/MTU	FR Growth, %		
				Case 1	Case 2	Case 3
47.1	0.83	**TSQ004**	48.12	1.08	1.14	1.17
		TSQ002	50.90	1.07	1.12	1.16
÷	÷	**TSQ024**	52.77	1.05	1.09	1.12
		TSL176	54.37	1.03	1.08	1.12
58.1	1.10	**TSQ022**	56.01	1.05	1.09	1.12

5.7 Fuel Rod Void Volume

The FR void volume change ($\Delta V_V/V_0$) calculated by the TU code for different fuel swelling and densification model parameters are listed in Table 5-4. The TU predicted data versus the measured ones are presented in Figure 5-6.

The obtained data of $\Delta V_V/V_0$ show:

- for the full-size fuel rods, the predicted $\Delta V_V/V_0$ value is ~13% on the average and does not significantly change when rod burnup grows from 48.12 GWD/MTU to 56.01 GWD/MTU;
- as a whole, the TU predicted data are underestimated by half (see Figure 5-6).

Table 5-4. Measured and TU Predicted Fuel Rod Void Volume Change.

Rod ID	Measured data		TU predicted data			
	Initial Void Volume, V_0, cm^3	EOL $\Delta V_V/ V_0$, %	Initial Void Volume, V_0, cm^3	EOL $\Delta V_V/ V_0$, %		
				Case 1	Case 2	Case 3
TSQ002	25.42	-30.0	27.94	-13.7	-15.7	-
TSQ004	-	-	27.94	-13.3	-15.2	-10.5
TSL076*	26.12	-26.9	-	-	-	-
TSL095*	25.91	-29.0	-	-	-	-
TSL176	25.32	-27.7	27.94	-14.2	-16.1	-11.6
TSQ022	37.22	-16.7	37.79	-11.2	-12.6	-9.3
TSQ024	-	-	38.22	-10.7	-11.7	- 8.4
TSQ103-C1	11.69	- 3.3	16.75	- 2.9	- 3.0	- 1.8
TSQ103-C2	7.79	-17.1	9.15	- 6.9	- 7.7	- 5.4
TSQ103-C3	4.00	-13.0	5.10	- 5.8	- 6.5	- 4.6
TSQ103-C4	3.94	-10.4	5.04	- 5.9	- 7.1	- 5.3
TSQ103-C5	3.98	-16.1	5.09	- 5.8	- 7.0	- 5.2
TSQ103-C6	3.96	- 9.4	5.07	- 5.9	- 7.1	- 5.7
TSQ103-C7	4.00	-13.8	5.10	- 5.8	- 6.9	- 5.2
TSQ103-C8	3.97	-11.8	5.07	- 5.8	- 7.3	- 4.8
TSQ103-C9	3.80	+ 0.8	5.59	- 2.8	- 0.3	- 1.9

* The data for these rods were taken from the PIE data-base [16] and used for comparison only.

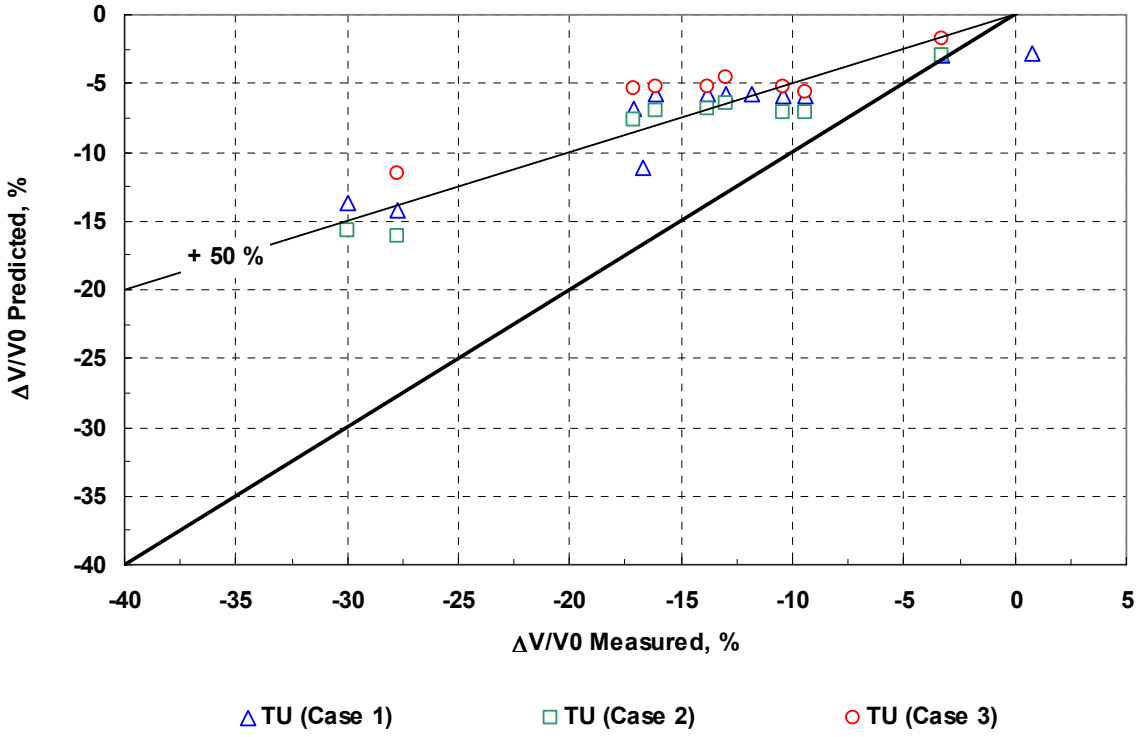

Figure 5-6. TU predicted fuel rod void volume change versus measured. (The void volume change, $\Delta V_V/V_0$, is determined as $(V_{EOL} - V_{BOL})/ V_{BOL}$).

5.8 Fission Gas Release and Rod Internal Pressure

The TU predicted fission gas release versus the measured is shown in Figure 5-7. The measured and the predicted data of gas Xe/Kr ratio are collected in Table 5-5. The presented data demonstrates:

- the TU calculated Xe/Kr ratio is in satisfactory agreement with the experimental data. The difference between the predicted and the measured data is ~ 4 % on the average;
- at the rod burnup less than 40 GWD/MTU, the predicted FGR is ~ 0.25 % and is close to the measured ones;
- at the rod burnup higher 40 GWD/MTU, the FGR values calculated based on the BE value of burnup threshold (85 GWD/MTU, *URGAS* model) are overestimated by the factor of ~ 3.

The FGR growth dynamic for the examined fuel rods is shown in Figure 5-8. As can be seen, for the fuel rods operated at steady-state up to a burnup of ~ 57 GWD/MTU the predicted FGR value is ~ 2.4 % on the average. It is 0.9 % higher than the PAD predicted data. The increase burnup threshold by 10% from the nominal value leads (i) to shift of the process of athermal FGR from 40 GWD/MTU to 45 GWD/MTU and (ii) to decrease in the fission gas release by 0.7 % on the average (see Figure 5-8, the dotted curve).

The predicted and the measured data for rod internal pressure are presented in Figure 5-9 and show:

- at the same burn-ups, the predicted RIP for the full-size FR with solid pellets is ~ 0.3 MPa higher than for the rod with annular pellets, which is close to the measured, 0.5 MPa ;
- the predicted RIP values for the full-size FRs with solid pellets lie on the lower boundary of the measured area and are overpredicted by 0.2 MPa for the rods with annular pellets;
- the predicted RIP values for the segmented TSQ103 fuel rod are overestimated by 0.2 MPa on the average.

Thus the predicted RIP values correlate with the experimental data. However, this correlation does not agree with the predicted data of rod void volume change, which are underestimated.

Table 5-5. Measured and TU Predicted Fission Gas Xe/Kr Ratio.

Rod ID	Xe/Kr Ratio	
	Measured data	TU predicted data
TSQ103-C1	10.5	10.63
TSQ103-C2	9.8	11.08
TSQ103-C3	10.2	11.06
TSQ103-C4	9.8	11.06
TSQ103-C5	10.2	11.05
TSQ103-C6	9.7	11.05
TSQ103-C7	10.6	11.04
TSQ103-C8	10.7	10.79
TSQ103-C9	11.0	8.18

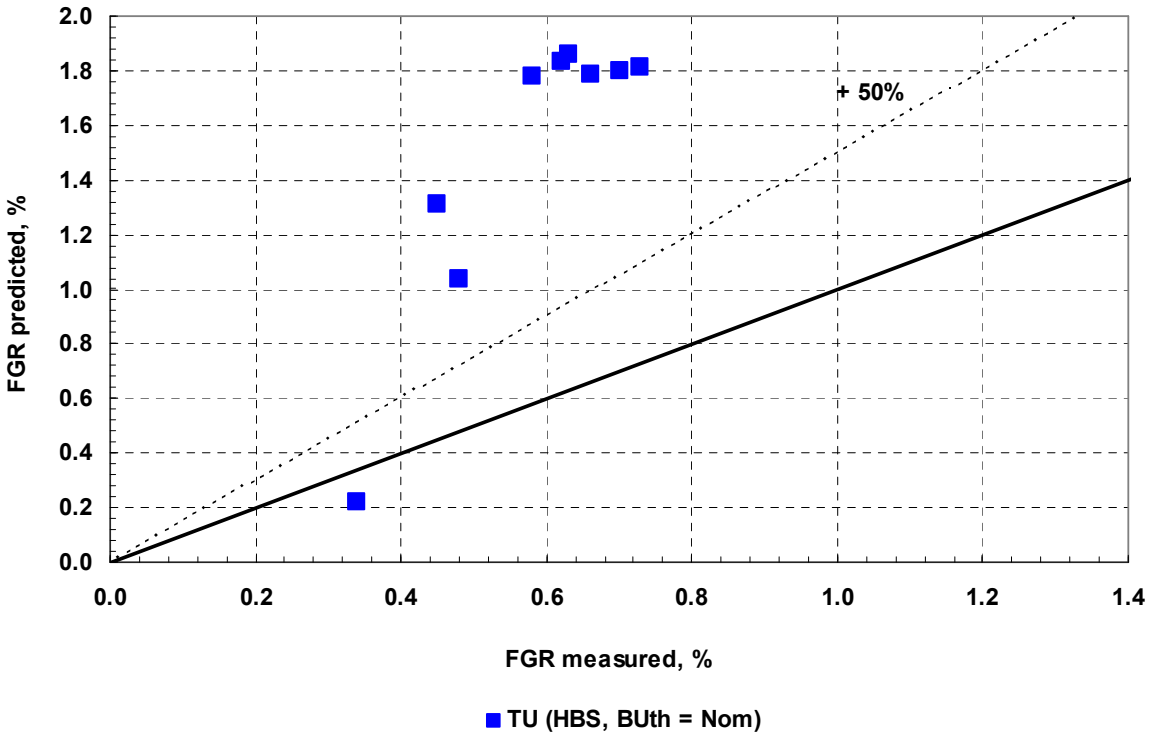

Figure 5-7. TU predicted fission gas release versus measured.

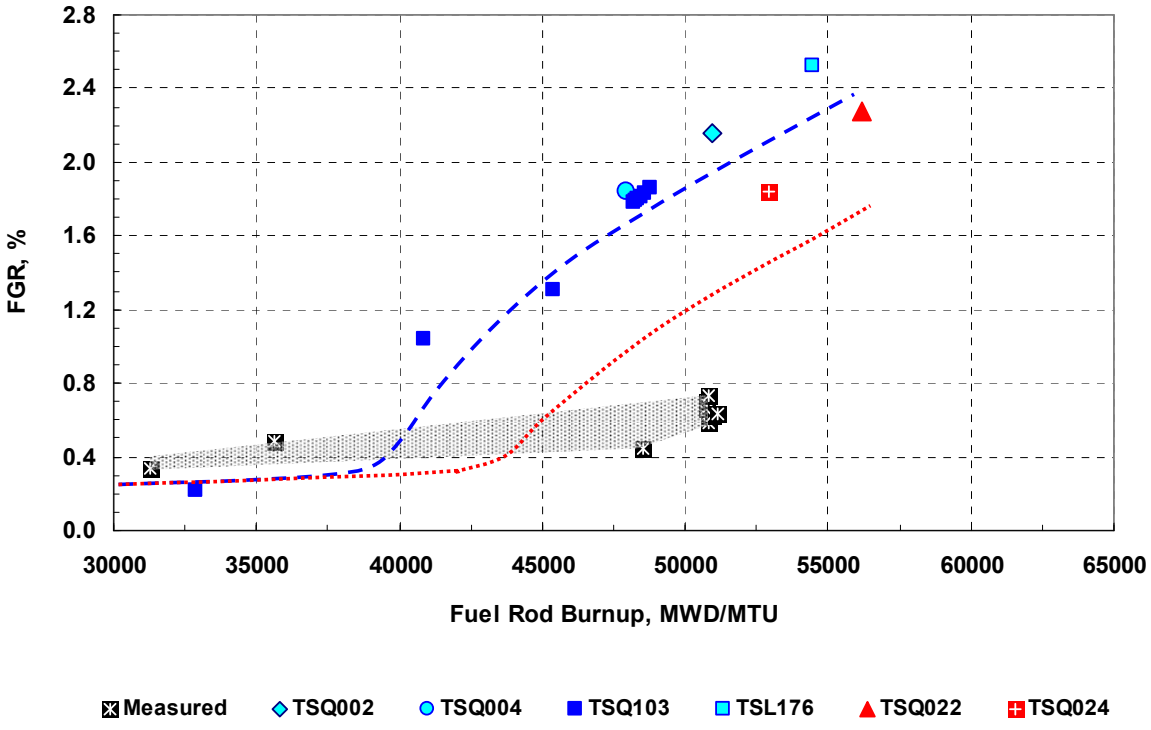

Figure 5-8. Measured and TU predicted FGR versus fuel rod burnup. (The dotted curve is built using the increased burnup threshold, 1.10 from the nominal).

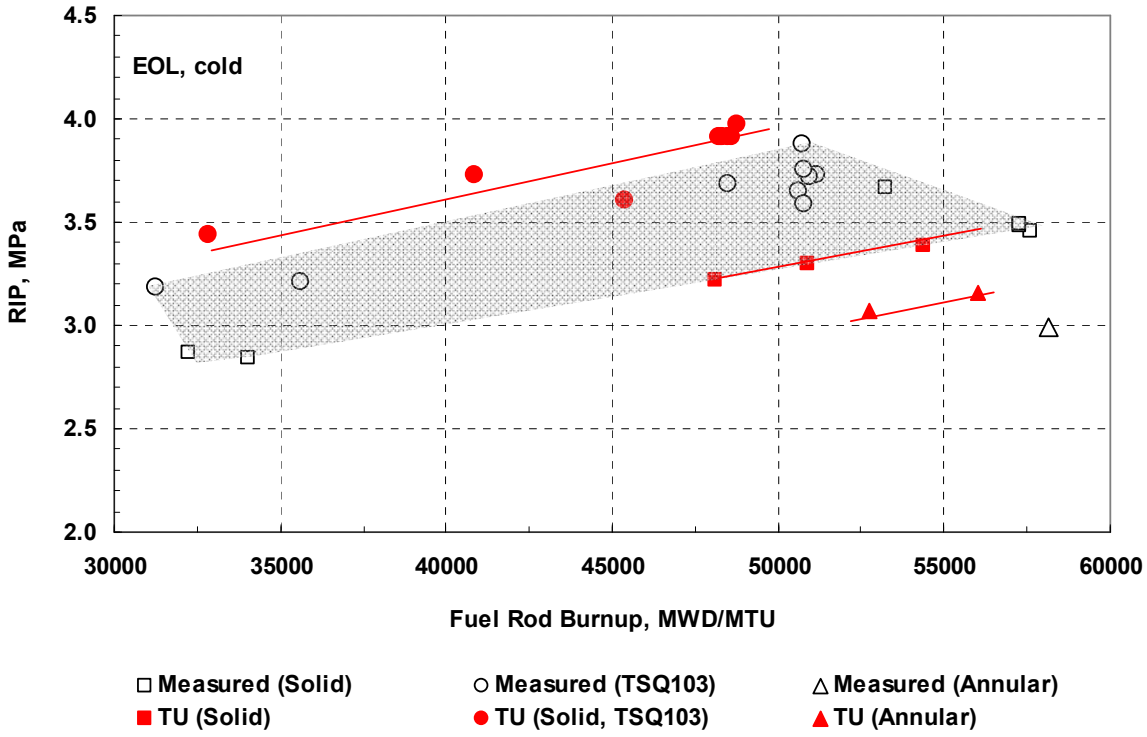

Figure 5-9. EOL measured and TU predicted rod internal pressure.

5.9 Conclusion

The prediction capability of the TRANSURANUS code for evaluating PWR fuel rod behavior under steady-state operation conditions has been assessed on the basis of experimental data from the *US-PWR 16×16 LTA Extended Burnup Demonstration Program*, which are available in the IFPE database of the OECD/NEA.

The analyses, which have focused on some integral quantities, have firstly pointed out that rod average burn-up predictions are continuously underestimated by ~3% on the average in the range of 40 ÷ 60 GWD/MTU. The peak oxide thickness for the cladding made of the standard Zr-4 alloy is underestimated by 25 mkm as a minimum. At the same time, for the examined rods the irradiation growth data are at the upper bound of the measured.

As concerns the cladding creepdown (cladding outer diameter change) at the end of life, a systematic over-prediction has been observed, when the BE model parameters (*denpor* = 0.020, *denbup* = 5000 GWD/MTU) were used. The increase in the fuel pore removable value (*denpor* = 0.012, *denbup* = 12000 GWD/MTU) provides better agreement with the experimental data. The same effect is also reached, when the axial anisotropy factor for fuel densification (*beta* = 0.1) is used with the BE model parameters. The absence of the measured data for fuel stack irradiation growth does not allow to make the exact conclusion about the axial anisotropy factor for fuel densification. Nevertheless, the increase in *denbup*- parameter up to~11000 GWD/MTU gives a positive integral effect on the fuel volume change and pellet-to-cladding interaction during irradiation.

The calculated rod void volumes are continuously underestimated by half of the measured. Since the predicted fuel volume change agrees with the measured, the underestimation of rod void volume can be related to overestimation of the rod growth.

The predicted gas Xe/Kr ratio is in satisfactory agreement with the measured data. As regards end-of-life FGR simulations, a 1.2 % overestimation with respect to the experimental data has been found. A 10% increase in the burnup threshold from the nominal value leads to an average 0.7 % decrease in the fission gas release. Nevertheless, the predicted FGR at high burnup lies within the commonly recognized acceptability band for the fuel rods operated at steady-state conditions.

REFERENCES

1. J. Killen, "IAEA Programme on Nuclear Fuel Cycle and Materials Technologies", Proc. of the 8-th International Conference on *WWER Fuel Performance, Modelling and experimental Support*, Burgas, Bulgaria, 26 Sept. – 2 Oct. 2009.
2. *Very-High Burn-ups in Light Water Reactor*, NEA/OECD No. 6224, 2006.
3. J.T.A. Roberts, *Structural Materials in Nuclear Power Systems*, Plenum Press, New York, 1981.
4. D.R. Olander, "Light Water Reactor Fuel Design and Performance", in Encyclopedia of Materials: *Science and Technology*, pp. 4490-4504, Elsevier Science Ltd., Oxford, 2001.
5. K. Lassmann, "TRANSURANUS: A Fuel Rod Analysis Code ready for Use", *Journal of Nuclear Materials*, vol. 188, pp. 295-302, 1992.
6. D. Lanning, C. Beyer and C. Painter, "*FRAPCON-3: Modifications to Fuel Rod Material Properties and Performancer Models for High-burnup Application*", NUREG/CR-6534, PNNL-11513, 1997.
7. M. Suzuki, "*Light Water Reactor Fuel Analysis Code FEMAXI-V (ver.1)*", JAERI-Data/Code 2000-030, 2000.
8. Y. Rashid, R. Dunhman and R. Montgomery, "*FALCON MOD01: Fuel Analysis and Licensing Code – New, Volume1: Theoretical and Numerical Bases*", ANA-04-0666 Report, EPRI, Palto Alto, CA, and ANATECH Corp., San Diego, CA, 2004.
9. P. Strijov, M. Valach, "*Description of the PIN-micro Innovation to the PINw99 code* ", UJV Draft-T,M, NRI Řež plc., CSFR August 1999.
10. A. Medvedev, S. Bogatyr and V. Kuznetsov, "*Code START-3: Initial Results of Blind Prediction of MOX Fuel Performance on Data Provided by the Halden Project*", Task Force on Reactor-based Plutonium, OECD/NEA, Paris, France, 2001.
11. Scheglov A., Proselkov V., "Code package to analyze behavior of the WWER fuel rods in normal regimes of operation. TOPRA-s code", Proc. of the 4-th International Conference on *WWER Fuel Performance, Modelling and experimental Support*, October 1–5 October 2001, Albena, Varna, Bulgaria. pp. 220–228
12. *PAD User Manual*, Code Version 10.5.2, Westinghouse Electric Company, 2005.
13. *Fuel Rod Design Procedure Manual*, Rev. 21, Westinghouse Electric Company, 2004.
14. *Safety Substantiation for the Use of Westinghouse Lead Test Assemblies in the SU NPP, Unit 3*, WEC-UNFQP-006, Rev. 3, Westinghouse Electric Company, February 2005.
15. J. Killeen, E. Sartori, M. McGrath, "FUMEX-III: A New IAEA Coordinated Research Project on Fuel Modelling at Extended Burnup", Proc. of the International Conference on *Water Reactor Fuel Performance* (WRFPM - Top Fuel 2009), Paper 2176, pp. 336-343, Paris, France, September 6-10, 2009.
16. IFPE, The Public Domain Database on Nuclear Fuel Performance Experiments for the Purpose of Code Development and Validation, International Fuel Performance Experiments (IFPE) Database, in: http://www.nea.fr/html/science/fuel/ifpelst.html, 2007.
17. K. Lassmann, P. Van Uffelen, A. Schubert, J. van de Laar, Cs. Győri, "TRANSURANUS Handbook", ('V1M1J09'), European Commission, Joint Research Centre, ITU, January 2009.

18. K. Lassmann, “URANUS - A Computer Programme for the Thermal and Mechanical Analysis of the Fuel Rods in a Nuclear Reactor”, *Nucl. Eng. Des.,* 45 (1978) 325.
19. K. Lassmann, “A Fast and Simple Iteration Scheme for the Temperature Calculation in a Fuel Rod”, *Nucl. Eng. Des*., 103 (1987) 211.
20. K. Lassmann, “The OXIRED Model for Redistribution of Oxygen in Nonstoichiometric Uranium-Plutonium Oxides”, *J. Nucl. Mater*., 150 (1987) 10.
21. K. Lassmann, T. Preußer, “The TEMPER Subcode System for Transient Temperature Calculation in Fuel Elements”, in: *Water Reactor Fuel Element Performance Computer Modelling,* by J. Gittus (Ed.), Applied Science Publishers LTD, Ripple Road, Barking, Essex, England, 1983, p. 297.
22. K. Lassmann, T. Preußer, “An Advanced Method for Transient Temperature Calculation In Fuel Element Structural Analysis”, *Nucl. Technol.*, 60 (1983) 406.
23. C. T. Walker, K. Lassmann, C. Ronchi, M. Coquerelle, M. Mogensen, “The D-COM Blind Problem on Fission Gas Release: The Predictions of the TRANSURANUS and Future Codes”, *Nucl. Eng. Des*., 117 (1989) 211.
24. K. Lassmann, C. O'Carroll, J. van de Laar, C. T. Walker, “The Radial Distribution of Plutonium in High Burnup UO_2 Fuels”, *J. Nucl. Mater*., 208 (1994) 223.
25. K. Lassmann, J. van de Laar, "The TRANSURANUS Gd Version", Proc. of IAEA RER/4/019, Licensing Fuel and Fuel Modelling Codes for WWER Reactors, Seminar on *Implementation of the WWER version of the TRANSURANUS Code and Its Application to Safety Criteria*, Sofia, Bulgaria, 7-11 December, 1998.
26. K. Lassmann, H. Benk, “Numerical Algorithms for Intragranular Fission Gas Release”, *J. Nucl. Mater.*, 280 (2000) 127.
27. K. Lassmann, "Numerical Algorithms for Intragranular Diffusional Fission Gas Rrelease Incorporated in the TRANSURANUS Code", Proc. of International Seminar on *Fission Gas Behavior in Water Reactor Fuels*, Cadarache, France, 26-29 Sept., 2000, p. 499.
28. P. Van Uffelen, A. Schubert, J. van de Laar, Cs. Győri, D. Elenkov, S. Boneva, M. Georgieva, S. Georgiev, Z. Hózer, D. Märtens, G. Spykman, C. Hellwig, Å. Nordstrøm, L. Luzzi, V. Di Marcello, L. Ott, "The Verification of the TRANSURANUS Fuel Performance Code - An Overview", INRNE (Ed.), Proc. of 7-th International Conference on *WWER Fuel Performance, Modelling and Experimental Support*, Albena, Bulgaria, 17-21 Sept. 2007.
29. P. Van Uffelen, Cs. Győri, A. Schubert, J. van de Laar, Z. Hozer, G. Spykman, “Extending the Application Range Of a Fuel Performance Code from Normal Operating to Design Basis Accident Conditions”, *J. Nucl. Mater*., 383 (2008) 137.
30. A. Schubert, P. Van Uffelen, J. van de Laar, C. T. Walker, W. Haeck, “Extension of the TRANSURANUS Burn-up Model”, *J. Nucl. Mater.*, 376 (2008) 1.
31. A. Schubert, Cs. Győri, J. van de Laar, S. Bznuni, T. Safaryan, T. Tverberg, J.-C. Kim, P. Van Uffelen, "Verification of the TRANSURANUS Burn-up Model for WWER Fuel and $(U,Gd)O_2$ Fuel", Proc. of the International Conference on *Physics of Reactors* (PHYSOR) "Nuclear Power: A Sustainable Resource", Interlaken, Switzerland, 14-19 Sept., 2008.

32. A. Schubert, Cs. Győri, J. van de Laar, P. Van Uffelen, S. Bznuni, T. Safaryan, "Extension of the TRANSURANUS Burn-up Model for Gd-Doped UO_2 Fuel in WWER Reactors", Proc. of 8-th International Conference on *WWER Fuel Performance, Modelling and Experimental Support*, Burgas, Bulgaria, 27 Sept.- 2 Oct., 2009.
33. *ASME International Steam Tables for Industrial Use*, IAPWS-IF97, ASME PRESS, Three Park Avenue, New York, 10016.
34. F. W. Dittus and L.M.K. Boelter, "Heat Transfer in Automobile Radiators of the Tubular Type", University of California - *Publications in Engineering*, 2, No. 13, p. 443-461 (1930).
35. NASA-TR-R-81, "Alignment Charts to Transport Properties, Viscosity, Thermal Conductivity and Diffusion Coefficients for Nonpolar Gases and Gas Mixtures at Low Density", 1960.
36. J. M. Gandhi and S. C. Saxena, "Correlated Thermal Conductivity Data of Rare Gases and Their Binary Mixtures at Ordinary Pressures," *J. Chem. Eng. Data* 13, No. 3, p. 357-361 (1968).
37. N. V. Tsederburg, *Thermal Conductivity of Gases and Liquids*, M.I.T. Press, 1965.
38. Y. Kosaka, "Thermal Conductivity Degradation Analysis of the Ultra High Burnup Experiment IFA-562", OECD Halden Reactor Project Report HWR-341, Halden, Norway, 1993.
39. *Westinghouse Improved Performance Analysis and Design Model (PAD 4.0)*, WCAP-15063-P-A, Rev. 1, July 2000.
40. NRC Regulatory Guide 1.126, "An Acceptable Model and Related Statistical Methods for the Analysis of Fuel Densification," Revision 1, March 1978.
41. A. D. Appelhans and J. A. Turnbull, "Measured Release of Radioactive Xenon, Krypton, and Iodine from UO_2 at Typical Light Water Reactor Conditions, and Comparison with Release Models," NUREG/CR-2298, November 1981.
42. D. D. Lanning, C. E. Beyer, C. L. Painter, "FRAPCON-3: Modifications to Fuel Rod Material Properties and Performance Models for High-Burnup Application", NUREG/CR-6534, Vol.1, PNNL-11513, October 1997.
43. B. Kanashov, S. Amosov, G. Lyadov, D. Markov *et al.*, "Change in Geometrical Parameters of WWER High Burnup Fuel Rods under Operation Conditions and Transient Testing", Proc. of 4th International Conference on *WWER Fuel Performance, Modelling and Experimental Support*, 1–5 October 2001, Varna, Bulgaria.
44. Smith, Jr., G. P., R. C. Pirek, H. R. Freeburn, and D. Schrire. 1994, "The Evaluation and Demonstration of Methods for Improved Nuclear Fuel Utilization", DOE/ET/34013-15, Combustion Engineering, Windsor, Connecticut.
45. F. J. Erbacher *et al.*, "Burst Criterion of Zircaloy Fuel Claddings in a Loss-of-Coolant Accident", *Zirconium in the Nuclear Industry*, 5-th Symposium, ASTM STP 754, p. 271-283, (1982).

ACKNOWLEDGEMENTS

The authors acknowledge J. Killeen from the IAEA and E. Sartori from the OECD/NEA for maintaining and developing the IFPE Database.

The authors also wish to thank the TRANSURANUS Developers Team at the Institute for Transuranium Elements in Karlsruhe and in particular P. Van Uffelen, A. Schubert, and J. van de Laar for their very helpful technical support.

APPENDIX A

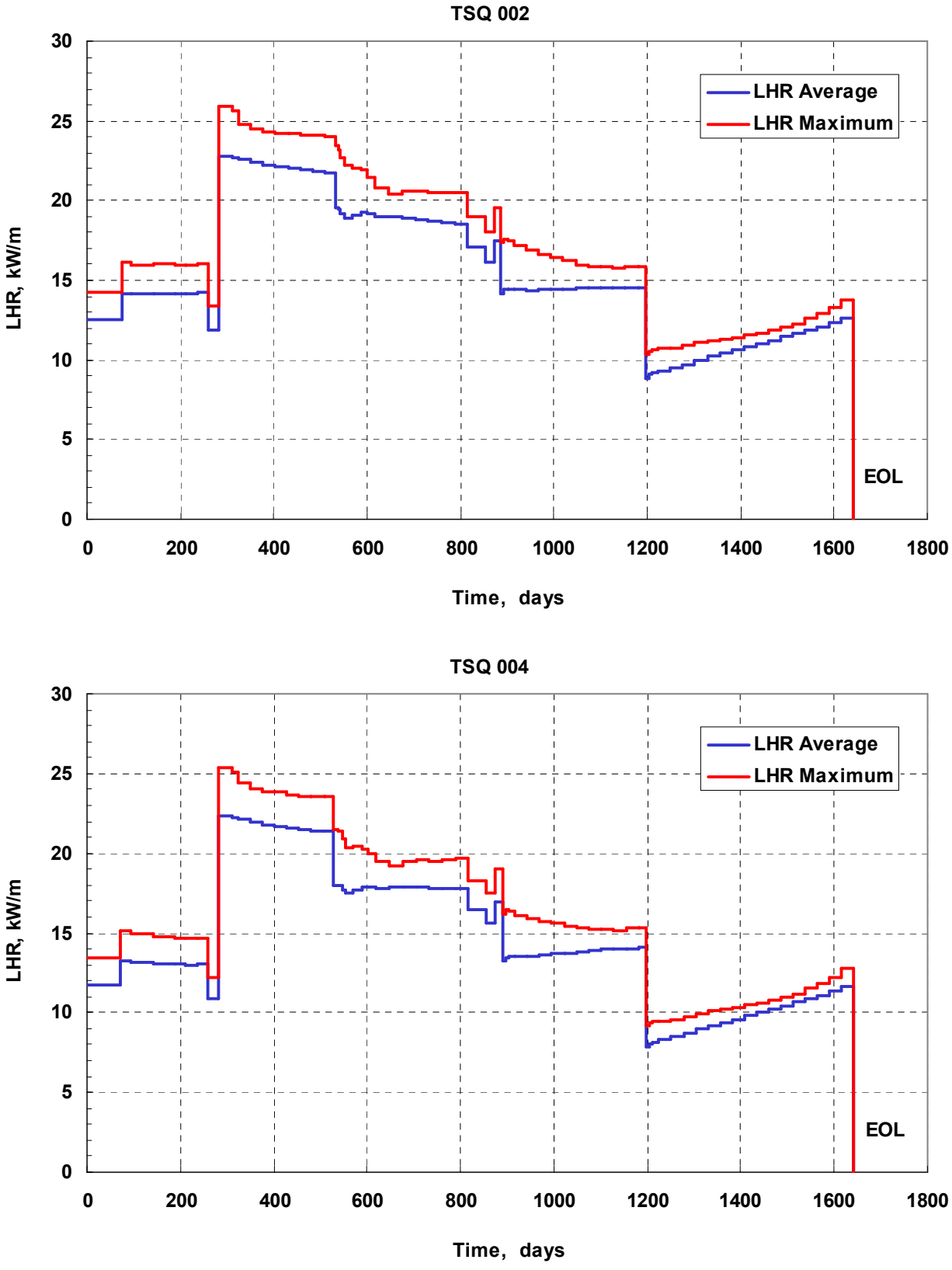

Figure 1A. Rod-average and rod maximum linear heat rates versus time for TSQ fuel rods operated for 5 cycles in ANO-2 PWR.

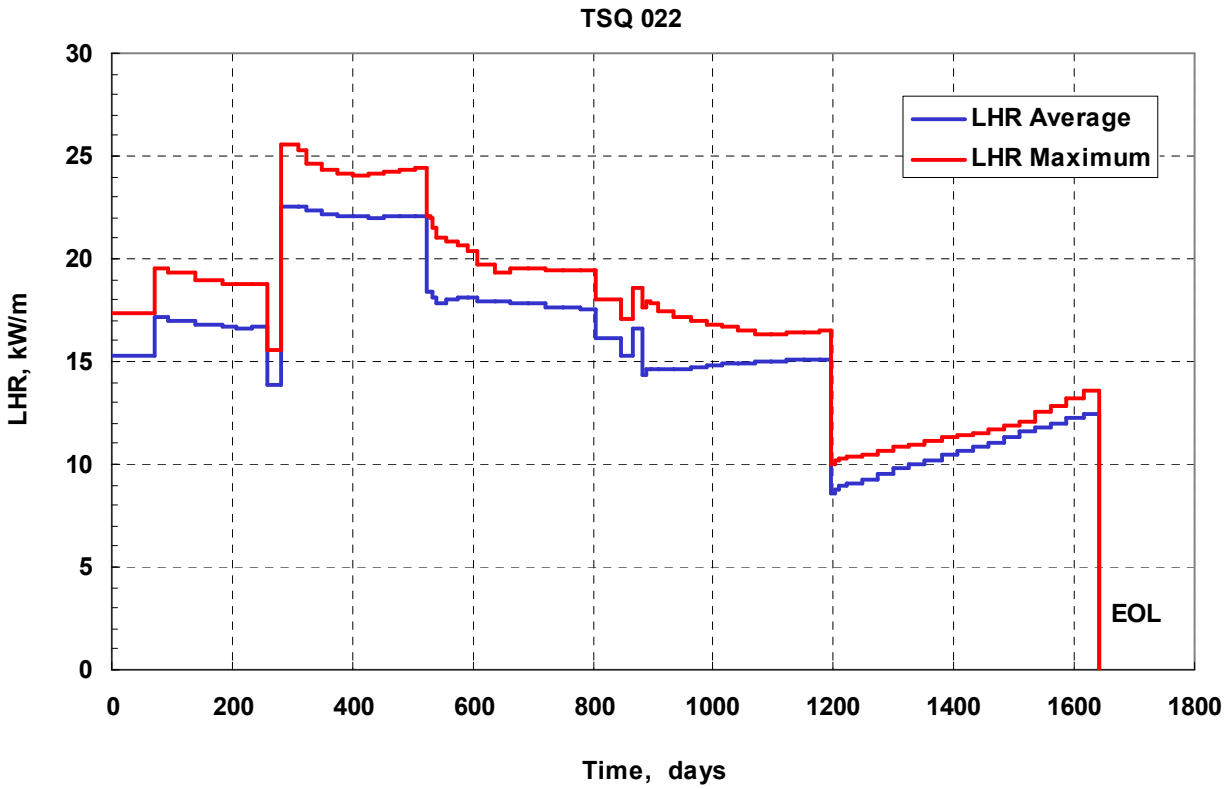

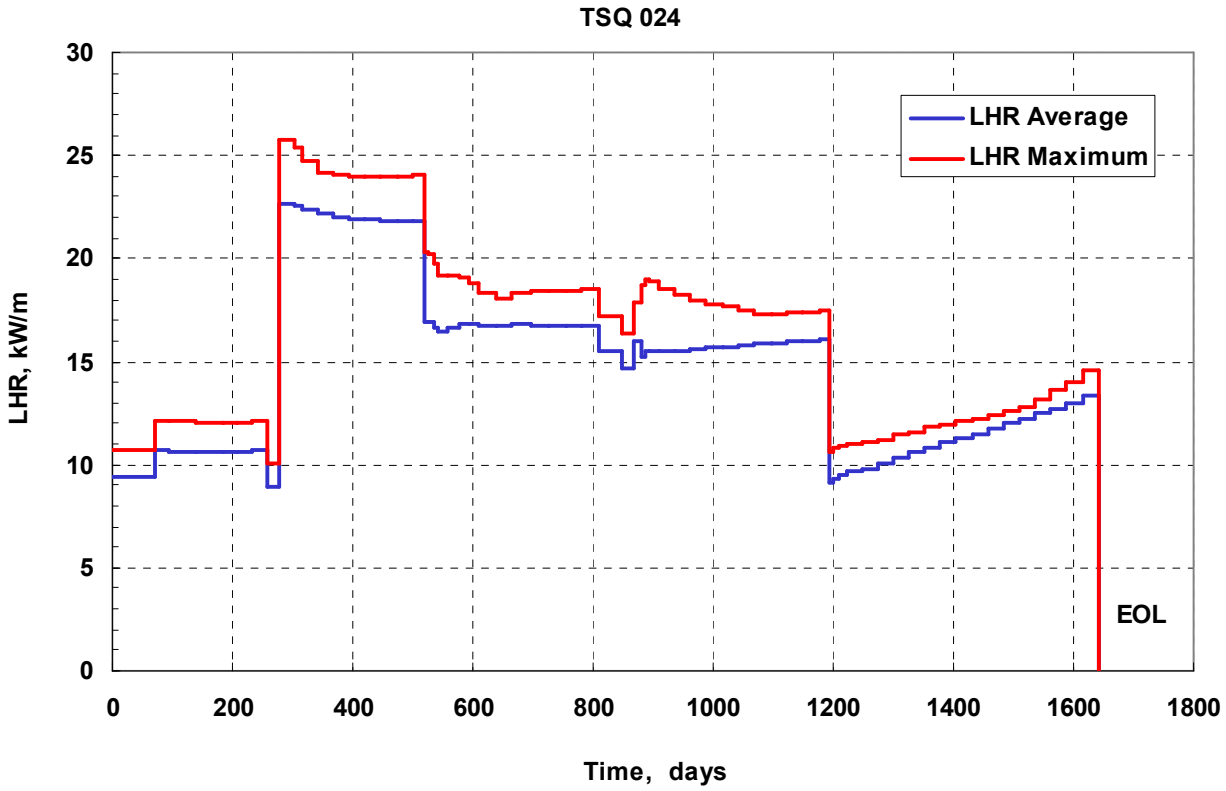

Figure 1A. Rod-average and rod maximum linear heat rates versus operation time for TSQ fuel rods operated for 5 cycles in ANO-2 PWR (continued).

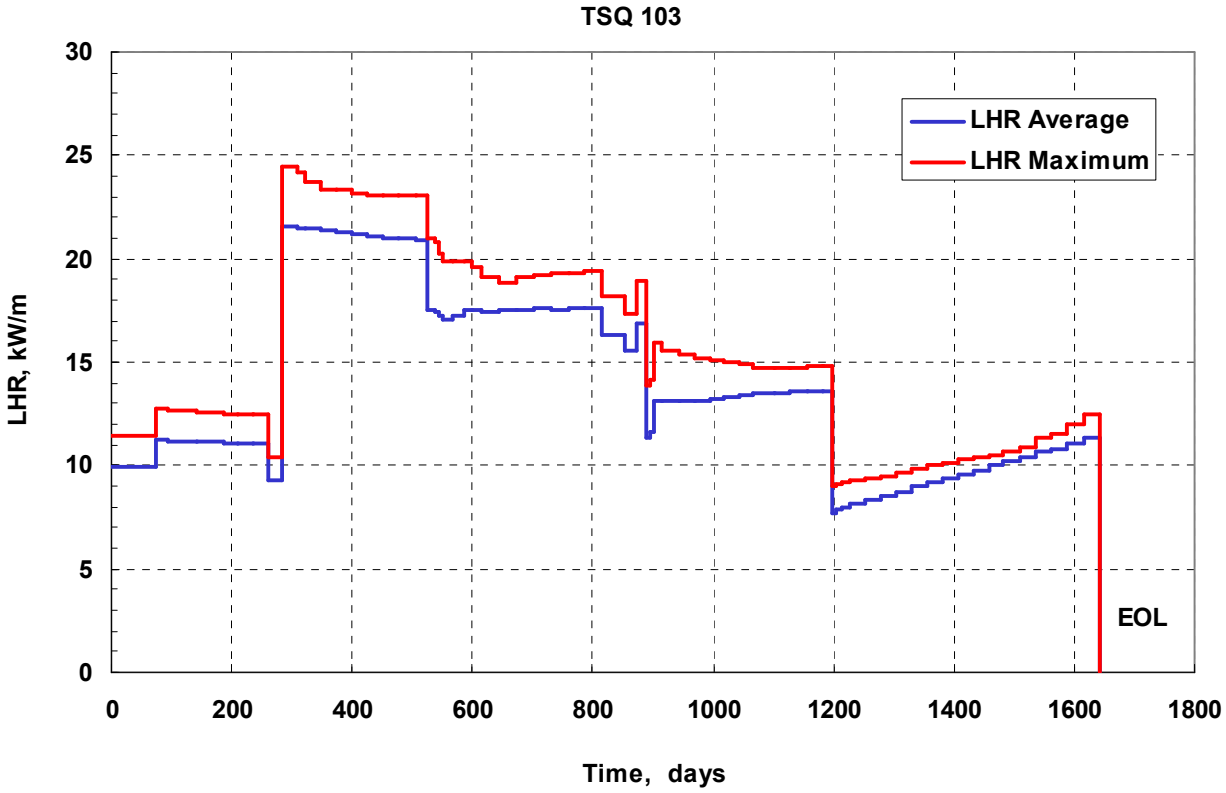

Figure 1A. Rod-average and rod maximum linear heat rates versus operation time for TSQ fuel rods operated for 5 cycles in ANO-2 PWR (continued).

Table A1. TRANSURANUS fuel rod models and model parameters used to simulate PWR fuel rod performances. ("Reference setting")

TU input variable	Value	Meaning
IKUEHL	0	The coolant temperature is calculated based on the coolant inlet temperature and mass flow rate.
IDENSI	2	Fuel densification is calculated by a simplified empirical model.
IRELOC	8	Fuel relocation is calculated by the modified *FRAPCON*-3.
ICRKPI	1	Crack volume is considered as free volume.
IXMODE	0	A no-slip condition is assumed for axial PCMI.
IZENKA	1	Central void formation is taken into account.
INTAXL	1	The gap conductance model takes into account the interaction between fuel and cladding.
ISLICE	1	The fuel stack is represented by slices (i.e. m_3 slices are treated).
IHYDD	1	The coolant channel is characterized by an equivalent hydraulic diameter.
IGRNSZ	1	Grain growth model of Ainscough and Olsen considered
FGRMOD	6	The intragranular fission gas release model *URGAS* (with the diffusion coefficients of Hj. Matzke (thermal) and a constant athermal diffusion coefficient) is considered
IDIFSOLV	0	FGR is solved by the *URGAS* algorithm.
IGRBDM	1	Intergranular fission gas release model (grain boundary gas saturation concentration of 1E-4 mol/m^2).
IHBS	2	High Burnup Structure is taken into account in the thermal and the mechanical analysis.
ICORRO	4	*MATPRO* cladding corrosion model for PWR conditions; thermal effect and the weakening of the cladding are considered.
MODPROP	4	Modification of specific material properties of the cladding and fuel is considered.
MODCLAD(2,3, 5÷20)	20	Standard PWR (LWR) settings for cladding material.
MODCLAD(1)	18	Creep anisotropy coefficients of Zirc-4 on the basis of [45].
MODCLAD(4)	18	Cladding strain due to swelling for stress relieved Zirc-4.
MODFUEL (1÷4; 7÷20)	20	Standard LWR settings for UO_2 fuel properties.
MODFUEL (6)	21	Fuel thermal conductivity according to Harding and Martin correlation for UO_2.
POR000	0.03535*	Total fuel pellet fabrication porosity (average)
DENPOR	0.020**	Porosity at the end of sintering
DENBUP	5000**	Burn-up at which sintering has stopped

* The fuel fabrication porosity of 0.03535, which provides the pellet density of 95.27% T.D. at BOL, is used as the basis for the examined LTA D040 fuel rods (see Chapter 3.6).

** The values of *denpor* and *denbup* are used as the basis in the reference setting.

APPENDIX B

1. Dish and Chamfer Pellet Volume Fraction

The dish and chamfer pellet volume fraction was calculated based on the dimensions from the figure presented below.

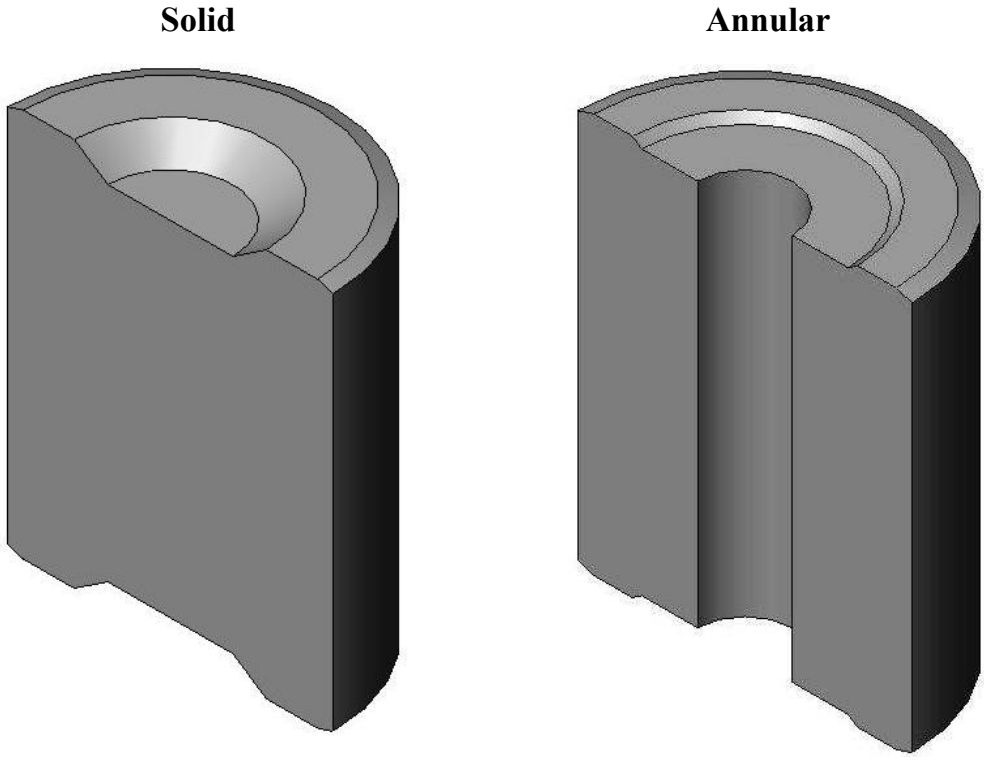

Pellet Axial Cross-section

Pellet Variable	***Value***		***Value***	
	inches	(mm)	**inches**	(mm)
CHAMF	*0.0050*	*(0.1270)*	*0.0050*	*(0.1270)*
CHAMFW	*0.0154*	*(0.3912)*	*0.0150*	*(0.3910)*
DISHDI	**0.1250**	(3.1750)	**0.2010**	(5.1054)
DISHDO	*0.1770*	*(4.4958)*	*0.2190*	*(5.5630)*
HDISH	*0.0183*	*(0.4648)*	*0.0063*	*(0.1588)*
DHOLE			**0.0920**	(2.3368)
HPLT	**0.3900**	(9.9060)	**0.3900**	(9.9060)
DP	**0.3250**	(8.2550)	**0.3250**	(8.2550)

where CHAMF - chamfer height; CHAMFW - chamfer width, which is defined as CHAMF/TAN(18^0), chamfer angle is ~18^0; DISHDI – dish inner diameter; DISHDO – dish outer diameter; HDISH – dish depth; DHOLE – pellet hole diameter; HPLT – pellet height; DP – pellet outer diameter. (It is noted, that the variables used in the fitting are in *italics*).

The pellet dish volume, V_{DISH}, is determined as:

$V_{DISH}\_SolPel. = 2\times[1/3\times\pi\times HDISH\times 1/4\times(DISHDO^2 + DISHDI^2 + DISHDO\times DISHDI)] =$
$= 6.6191E\text{-}04\ in^3;$

$V_{DISH}\_AnnPel. = 2\times[1/3\times\pi\times HDISH\times 1/4\times(DISHDO^2 + DISHDI^2 + DISHDO\times DISHDI) -$
$1/4\times\pi\times DHOLE^2\times HDISH] = 3.5012E\text{-}04\ in^3.$

The pellet chamfer volume, V_{CHAMF}, is determined as:

$V_{CHAMF} = 2\times\pi\times CHAMF\times CHAMFW\times(1/2\times DP - 1/3\times CHAMFW) = 7.6135E\text{-}05\ in^3;$

The dish and chamfer pellet volume fraction, V_{VOID}, is determined as:

$V_{VOID} = (V_{DISH} + V_{CHAMF})/V_{PELLET} = (V_{DISH} + V_{CHAMF})/(1/4\times\pi\times DP^2\times HPLT) =$

≈ 0.0228 and 0.0131 for solid and annular pellets, respectively.

2. Pellet Volume and Weight

The pellet volume, V_{PEL}, is determined as:

$V_{PEL}\_SolPel. = (1 - V_{VOID})\times(1/4\times\pi\times DP^2\times HPLT) = 3.1616E\text{-}02\ in^3\ (0.5181\ cm^3)$

$V_{PEL}\_AnnPel. = (1 - V_{VOID} - DHOLE^2/DP^2)\times(1/4\times\pi\times DP^2\times HPLT) = 2.9335E\text{-}02\ in^3\ (0.4807\ cm^3)$

The calculated solid pellet volume of $0.5181\ cm^3$ lies within the range of pellet volumes measured for the solid pellets of a segmented TSQ103 fuel rod (see Table A1, "*US-PWR 16x16 LTA Extended Burnup Demonstration Program*", Summary File, Rev. 1, [16]):

- #C1 - $0.5173\ cm^3$ (= $26.90\ cm^3$/ 52 pellets);
- #C2 - $0.5154\ cm^3$ (= $31.44\ cm^3$/ 61 pellets);
- #C3-C8 - $0.5225\ cm^3$ (≈ $14.63\ cm^3$/ 28 pellets);
- #C9 - $0.5233\ cm^3$ (= $9.42\ cm^3$/ 18 pellets).

For the pellet density of $10.442\ g/cm^3$ (95.27 % T.D.), which is used for fuel performance evaluation, the pellet weigh is:

$W\_SolPel. = 10.442\ g/cm^3\times 0.5181\ cm^3 = 5.410\ g;$
$W\_AnnlPel. = 10.442\ g/cm^3\times 0.4807\ cm^3 = 5.019\ g.$